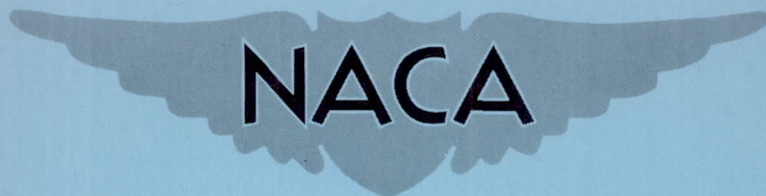


~~CONFIDENTIAL~~

Copy 320
RM H55H10

NACA RM H55H10



RESEARCH MEMORANDUM

FLIGHT MEASUREMENTS OF THE DYNAMIC LATERAL
AND LONGITUDINAL STABILITY OF THE BELL X-5
RESEARCH AIRPLANE AT 58.7° SWEEPBACK

By Edward N. Videan

High-Speed Flight Station
Edwards, Calif.

CLASSIFICATION CHANGED TO UNCLASSIFIED

AUTHORITY: NACA RESEARCH ABSTRACT NO. 97

DATE: FEBRUARY 24, 1956

WHL

CLASSIFIED DOCUMENT

This material contains information affecting the National Defense of the United States within the meaning of the espionage laws, Title 18, U.S.C., Secs. 793 and 794, the transmission or revelation of which in any manner to an unauthorized person is prohibited by law.

**NATIONAL ADVISORY COMMITTEE
FOR AERONAUTICS**

WASHINGTON

October 6, 1955

~~CONFIDENTIAL~~

NATIONAL ADVISORY COMMITTEE FOR AERONAUTICS

RESEARCH MEMORANDUM

FLIGHT MEASUREMENTS OF THE DYNAMIC LATERAL
AND LONGITUDINAL STABILITY OF THE BELL X-5
RESEARCH AIRPLANE AT 58.7° SWEEPBACK

By Edward N. Videan

SUMMARY

An investigation has been made of the dynamic stability of the Bell X-5 research airplane at 58.7° sweepback and at altitudes of 40,000 feet and 25,000 feet over a Mach number range of 0.50 to 0.97.

The results of this investigation show that the longitudinal oscillatory motions are well damped over the entire Mach number range except for residual oscillations resulting principally from engine gyroscopic coupling with the lateral oscillatory mode. The lateral oscillatory mode is moderately well damped except for nonlinear damping characteristics above a Mach number of 0.80. The damping is high for large amplitudes but for sideslip angles of less than 2° the damping is poor. The airplane is highly sensitive to small inadvertent control motions which produce apparently undamped small amplitude oscillations in the Mach number range above $M = 0.80$.

By U. S. Military Specifications, the lateral oscillation is marginal except in the nonlinear damping range where it is definitely unsatisfactory.

The longitudinal and lateral frequency-response characteristics were obtained and some coupling effects were noted. Longitudinal frequency-response calculations were characterized by adjacently located double peaks in amplitude ratio. This behavior is satisfactorily explained by theoretical calculations of frequency response involving engine gyroscopic coupling to the lateral mode. Lateral frequency responses showed some dependence on the direction of the initial disturbance.

INTRODUCTION

The Bell X-5 research airplane was designed primarily for investigating the effects of wing sweep angle on transonic airplane characteristics. Accordingly, this airplane incorporates a wing which has sweepback variable in flight from 20° to 58.7° . As part of the research program, flight measurements have been made with the X-5 airplane to determine the longitudinal and lateral dynamic stability characteristics over a Mach number range of 0.50 to 0.97 at an altitude of about 40,000 feet and with a wing sweep angle of 58.7° . Flight measurements have also been made at 25,000 feet to determine altitude effects. This paper presents the longitudinal and lateral dynamic characteristics in terms of P , $T_{1/2}$ at altitudes of 40,000 feet and 25,000 feet. Some of the longitudinal stability derivatives are also presented for these altitudes. The longitudinal and lateral frequency responses are given for the tests at an altitude of 40,000 feet.

SYMBOLS

b wing span, ft

C_L lift coefficient, L/qS

$$C_{L\alpha} = dC_L/d\alpha$$

$$C_{L\delta_e} = dC_L/d\delta_e$$

C_m pitching-moment coefficient about airplane center of gravity

$$C_{m\alpha} = dC_m/d\alpha$$

$$C_{m\dot{\alpha}} = \frac{dC_m}{d\left(\frac{\dot{\alpha}\bar{c}}{2V}\right)}$$

$$\bar{C}_{m\dot{\alpha}} = \frac{\bar{c}}{2V} C_{m\dot{\alpha}}$$

$$C_{m\delta_e} = dC_m/d\delta_e$$

$$C_{m\dot{\theta}} = \frac{dC_m}{d\left(\frac{\dot{\theta}\bar{c}}{2V}\right)}$$

$$\bar{C}_{m\dot{\theta}} = \frac{\bar{c}}{2V} C_{m\dot{\theta}}$$

$C_{m\dot{\psi}}$ rate of change of pitching moment due to engine gyroscopic moment with precessional yawing velocity

C_{N_A} normal-force coefficient

$C_{n\dot{\theta}}$ rate of change of yawing moment due to engine gyroscopic moment with precessional pitching velocity

$$C_{n\dot{\psi}} = dC_n/d\dot{\psi}$$

$$C_{n\dot{\psi}} = dC_n/d\dot{\psi}$$

$C_{1/2}$ cycles for oscillation to damp to one-half amplitude

$C_{1/10}$ cycles for oscillation to damp to one-tenth amplitude

c chord, ft

\bar{c} mean aerodynamic chord, ft

D d/dt , differential operator with respect to time

g acceleration due to gravity, ft/sec^2

h_p pressure altitude, ft

I_Y moment of inertia about Y-body axis through center of gravity, slug-ft²

I_Z moment of inertia about Z-body axis through center of gravity, slug-ft²

L lift, lb

M Mach number

m mass, slugs

n	normal acceleration, g units
P	period of oscillation, sec
q	dynamic pressure, $\frac{1}{2}\rho V^2$, lb/sq ft
S	area of wing, sq ft
$T_{1/2}$	time for oscillation to damp to one-half amplitude, sec
t	time, sec
V	velocity, ft/sec
v_e	equivalent side velocity, $\frac{\beta V}{57.3} \sqrt{\sigma}$, ft/sec
α	angle of attack, deg or radians
$\dot{\alpha}$	$d\alpha/dt$, radians/sec
β	angle of sideslip, deg
$ \beta $	double amplitude of β in oscillatory mode
δ_a	single aileron position, deg
δ_e	elevator position, deg or radians
δ_r	rudder position, deg
θ	pitch angle, radians
$\dot{\theta}$	pitching angular velocity, $d\theta/dt$, radians/sec
ρ	air density, slugs/cu ft
σ	air density ratio
ϕ	phase angle, deg
φ	rolling angle, deg
$\dot{\varphi}$	rolling angular velocity, radians/sec
$ \varphi $	double amplitude of φ in oscillatory mode

ψ	angle of yaw, radians
$\dot{\psi}$	yawing angular velocity, $d\psi/dt$, radians/sec
ω	frequency, radians/sec

$$\frac{|\phi|}{|v_e|} = \frac{|\phi| 57.3}{|\beta| \sqrt{v\sigma}}$$

AIRPLANE AND INSTRUMENTATION

A three-view drawing of the X-5 research airplane is shown in figure 1(a), and a photograph is presented in figure 1(b). Pertinent physical characteristics are described in table I.

Standard NACA internal recording instruments were used to measure airspeed, altitude, normal acceleration, pitching, rolling, and yawing angular velocities, angle of attack, angle of sideslip, and control surface position. All recordings were synchronized by a common timer.

The angular velocities were measured by rate gyros with accuracies of 0.5 percent of instrument full scale. These instruments have the following ranges and dynamic characteristics:

Angular velocity	Range, radians/sec	Natural frequency, cps (approx.)	Damping (approx.)
Pitch	± 0.5	9.0	0.65 critical
Yaw	± 1.0	13.5	0.65 critical
Roll	± 3.0	17.0	0.65 critical

The flow direction recorders were vane-type pickups mounted on the nose boom. The undamped natural frequency is about 8 cycles per second and the damping ratio is approximately 0.7.

Rudder, aileron, and elevator positions were measured by transmitters linked directly to the control surfaces. The frequency response of the transmitter-recorder system has been measured and found to be flat to 20 cycles per second over the amplitude range of the control movements presented.

Airspeed was measured from a calibrated nose-boom installation. The accuracy of the airspeed calibration is ± 0.01 in Mach number.

TESTS

The data were obtained from the transient oscillation of the airplane in response to rudder pulses, elevator pulses, and aileron pulses. The rudder pulse magnitudes were 5° to 12° , the elevator pulse magnitudes were 4° to 9° , and the aileron pulse magnitudes were 20° to 28° . The time duration of all pulses was 0.3 second to 1.0 second. At all times the pilot attempted to have the pulse terminate with the control surface in its initial position and to hold the control surface fixed for the duration of the maneuver. Generally all other controls were also held constant throughout the maneuver. The pulses and resulting transient oscillations at pressure altitudes of 40,000 feet and at Mach numbers below 0.93 were obtained for initial 1 g trim flight conditions. To obtain data at speeds greater than $M = 0.93$ it was necessary to dive the airplane at angles up to 10° . However, these dive angles were sufficiently small so that the change in altitude would have negligible effect on the oscillation. A smaller number of pulses were made at 25,000 feet to investigate altitude effects. Figure 2 presents the average normal-force coefficient C_{NA} as a function of Mach number for all pulses at both 25,000 feet and 40,000 feet.

RESULTS AND DISCUSSION

Longitudinal Stability

Figure 3 presents representative time histories of the X-5 airplane transient-longitudinal response to an elevator pulse at 40,000 feet. These time histories were chosen to cover the important parts of the Mach number range of the flight test measurements. Figure 3 shows that the longitudinal motions immediately following the elevator pulse damp quickly over the entire Mach number range. However, the time histories also show that the longitudinal oscillations induce a lateral-directional mode of oscillation which in turn affects the initial transient-longitudinal oscillation. This coupling will be discussed later in conjunction with lateral stability and frequency response.

Figure 4 presents the variations with Mach number of the period, time to damp to one-half amplitude, and cycles to damp to one-tenth amplitude for the longitudinal response of the airplane to an elevator pulse. These measurements were obtained from $\dot{\theta}$ over the first part of the transient oscillation immediately following the cessation of control movements. This portion of the curve was chosen for making the measurements in an attempt to minimize the effects of cross coupling with the lateral mode. It is impossible to exclude these effects entirely because, as the time histories show (fig. 3), the lateral-directional mode is disturbed almost as soon as the longitudinal mode

is disturbed. This condition makes the measurement of $T_{1/2}$ particularly difficult and casts some doubt on the validity of the measurements of both period and time to damp to one-half amplitude, but it is considered to be the best approximation to the true uncoupled longitudinal period and damping. The data at 40,000 feet (fig. 4) show that the period varies smoothly with Mach number, decreasing gradually from about 2.0 seconds at $M = 0.56$ to about 1.5 seconds at $M = 0.92$. Above this speed the period drops more sharply, reaching 1.1 seconds at $M = 0.97$. The data at 25,000 feet show that the period decreases by about 20 percent to 26 percent of the value at 40,000 feet. The approximate theoretical change with altitude is 29 percent, based upon the approximation that the ratio of the periods at the two altitudes is equal to the square root of the inverse ratio of dynamic pressure.

The damping at 40,000 feet changes only slightly with Mach number, the time to damp to one-half amplitude varying from near 1.0 second at $M = 0.55$ to near 0.5 second at $M = 0.97$. This results in a variation with Mach number of the number of cycles to damp to one-tenth amplitude as shown in figure 4. At 25,000 feet $T_{1/2}$ and $C_{1/10}$ show only small differences from the data at 40,000 feet.

Figure 5 presents the variation of the longitudinal stability derivatives $C_{m\alpha}$ and $C_{m\dot{\theta}} + C_{m\dot{\alpha}}$ with Mach number for the two test altitudes. These derivatives were calculated from the period and damping by the relations:

$$C_{m\alpha} = - \frac{I_Y}{qS\bar{c}} \left[\left(\frac{2\pi}{P} \right)^2 + \left(\frac{0.693}{T_{1/2}} \right)^2 \right]$$

$$C_{m\dot{\theta}} + C_{m\dot{\alpha}} = \frac{8I_Y}{\rho S V \bar{c}^2} \left(C_{L\alpha} \frac{\rho V S}{4m} - \frac{0.693}{T_{1/2}} \right)$$

The lift-curve slope used in the computation of $C_{m\dot{\theta}} + C_{m\dot{\alpha}}$ was obtained from flight measurements as presented in reference 1. Reference 2 shows that above $M = 0.6$ and below the pitch-up boundary (ref. 3) the X-5 airplane possesses two static stability regions and a transitional region which are dependent upon Mach number and C_{N_A} . These regions (low lift - decreased stability, transitional stability, moderate lift - increased stability) are marked in figure 2. It may be seen that most of the pulse maneuvers performed at 40,000 feet are in or near the transitional region, whereas the maneuvers performed at 25,000 feet are in a region of constant though decreased stability. Values of $C_{m\alpha}$ (fig. 5),

calculated from the data at 40,000 feet are, therefore, more subject to scatter than the data at 25,000 feet. Figure 5 shows that the agreement of $C_{m\alpha}$ calculations for the two altitudes is not perfect. It appears that closest agreement is obtained between $M = 0.8$ and $M = 0.9$ where the average C_{NA} at the two altitudes is on the same side of the transitional region of stability (fig. 2).

The values of $C_{m\dot{\theta}} + C_{m\dot{\alpha}}$, also presented in figure 5, show some scatter which is common to this method of obtaining the derivative. The scatter is possibly aggravated by the aforementioned effects of coupling on the determination of $T_{1/2}$. However, the difference between the data at 40,000 feet and 25,000 feet is larger than the average scatter.

Lateral Stability

During the early flights at 58.7° sweepback, the pilots complained and records showed that the airplane oscillated almost continuously in the lateral-directional mode at small amplitudes, particularly at Mach numbers above 0.80. An investigation was made to determine if this poor lateral dynamic behavior was affected by the magnitude of the disturbance and if the motions resulting from large disturbances were stable.

Accordingly, rudder pulses of large amplitude were performed at 40,000 feet over the Mach number range from 0.52 to 0.96 and rudder pulses of varying amplitude were performed at Mach numbers between 0.8 and 0.9. Throughout each pulse of the latter group the stick was held fixed by a mechanical stop to prevent inadvertent stick movements.

Figure 6 presents typical time histories at 40,000 feet of the transient response of the X-5 airplane to rudder pulses over the Mach number range tested. In the measurement of damping from such time histories it was noted that $T_{1/2}$ at large amplitude depended somewhat on the direction of the initial disturbance. Also, though good damping as measured by $T_{1/2}$ was usually present at large amplitudes, it was observed that the damping would decrease with decreasing amplitude resulting in near zero damping at small amplitudes (fig. 7). To show the nonlinear effect, the damping was measured as shown by the hypothetical curve in figure 8. The "large amplitude" range and "small amplitude" range were separated at about $|\beta| = 2^\circ$. The period and damping for these two portions of the oscillations are shown in figure 9. The characteristics of the residual oscillation are presented in figure 10. Figure 9 shows that the period varies smoothly with Mach number, ranging from 2.8 seconds at $M = 0.52$ to about 1.3 seconds at $M = 0.96$. The damping measured over the large amplitude portion of the oscillation also shows a smooth and fairly consistent variation up to $M \approx 0.75$.

For higher Mach numbers, despite scatter, there is a noticeable separation between values of $T_{1/2}$ for large amplitude and small amplitude. This behavior appears to continue to the highest Mach numbers tested. The cycles to damp to one-half amplitude show a similar trend. In general, the damping of large amplitude lateral motion is good throughout the Mach number range.

The damping measured for small amplitudes (fig. 9), however, shows appreciably large variations with Mach number. The low amplitude damping begins to vary noticeably from the large amplitude damping at a Mach number of about 0.83 and reaches a maximum $T_{1/2}$ value about double the large amplitude $T_{1/2}$ at $M \approx 0.86$ to $M \approx 0.88$. Above $M \approx 0.93$ the low amplitude damping increases rapidly and again generally approaches the large amplitude damping. The cycles required to damp generally follow a variation similar to the time required to damp. This variation between small amplitude and large amplitude damping thus defines a region of nonlinear damping extending from about $M \approx 0.80$ to the test limit. However, the pilots report that the airplane apparently regains much of its damping in the small amplitude range above $M = 0.93$.

Included as points in figure 9 are the results of the series of rudder pulses in the Mach number range of 0.80 to 0.90 in which rudder deflections of various amplitudes were made. As shown in the figure, points for large and small oscillatory amplitude as previously defined are fairly well grouped. The scatter existing in these two groups could not be identified with the size of the rudder pulse. Therefore it is concluded that the magnitude of the rudder disturbance does not directly affect the damping to any extent, except as it affects the initial amplitude of the oscillations.

Figure 10 presents the amplitude of the residual undamped oscillation of the lateral transient oscillation for the stick held fixed with the mechanical stop as well as with simple manual restraint. These data were obtained primarily at the end of the transient oscillations. However a few points, mostly those of the higher amplitude, are taken from undamped self-excited oscillations such as those of figure 7. These data show that with the stick restrained by the mechanical stop the residual oscillation amplitude reached a maximum of 0.3° as compared with a maximum residual amplitude in sideslip of about 2.5° when the stick is held manually. From these tests it would appear that small aileron movements are the major cause of the residual lateral oscillation. Figure 7 does not appear to bear out this conclusion since all controls are fixed within the limits of the recorder as noted in figure 7. However, as stated in the following pilots' comments, any small disturbances such as gusts may initiate these oscillations. It will be noticed that the amplitude of the residual oscillation and the nonlinear damping characteristics follow the same variation with Mach number. Therefore, it would

appear that outside the nonlinear damping range, below $M \approx 0.80$, the higher damping at small amplitude of oscillation keeps the small disturbances from causing a continuous oscillation.

Figure 11 presents the period and damping for the response to rudder pulses at 25,000 feet. It may be noted from the figure that the cycles to damp to one-half amplitude show about the same variations as shown by the large amplitude points at 40,000 feet. However, at the lower altitudes and lower C_{NA} (fig. 2) the nonlinear damping effects have disappeared and the damping remains constant with amplitude over the whole amplitude range.

The data shown in figures 9 to 11 are in substantial agreement with the pilots' comments on the dynamic stability of the X-5 airplane. NACA pilots who have flown the X-5 airplane feel that the Mach number range of 0.85 to 0.92 is dynamically less stable than at speeds above this range. The pilots agree that in the least stable region the airplane is subject to almost continuous lateral oscillations of low amplitude with zero damping, similar to the time history of figure 7. The pilots report that gusts, changes in power setting, or small control motions initiate these undamped oscillations.

Figures 12 and 13 present the new Military Specifications for dynamic lateral stability (ref. 4) and the recently superseded U. S. Air Force criteria for dynamic lateral stability (ref. 5), respectively. The new Specifications (fig. 12) relate the reciprocal of the number of cycles to damp to one-half amplitude to the ratio of roll angle to side velocity, which is given by $\frac{|\phi|}{|v_e|} = \frac{|\phi|}{|\beta|} \frac{57.3}{V\sqrt{\sigma}}$. The value of ϕ was obtained by integrating the roll velocity, whereas β was measured directly from a flow direction recorder. The points presented are calculated for the various damping regions of the transient oscillation previously mentioned. According to the new Specifications, some points fall into the satisfactory region and others into the unsatisfactory region. At the lowest Mach number range the points fall in the satisfactory region but are near the border of the unsatisfactory region. In the other speed ranges the majority of points fall into the unsatisfactory region.

The superseded Air Force criteria (ref. 5) is presented in figure 13. A representative number of points over the Mach number range have been plotted in this figure. The majority of points fall into the unsatisfactory region but are fairly close to the boundary between the unsatisfactory and satisfactory region.

It will be noticed that by both the old and new criteria the dynamic lateral stability of the X-5 airplane is predominantly unsatisfactory.

In evaluating the airplane, the pilots feel that the lateral dynamic stability characteristics are unsatisfactory, but tolerable, except in that portion of the speed range where the damping becomes noticeably nonlinear. In this region the low damping at small amplitude coupled with a large roll-to-sideslip ratio makes the behavior intolerable.

Coupling of Oscillatory Motions

As shown by the time-history plots (figs. 3, 6, and 7), there is coupling between the lateral and longitudinal oscillatory modes. In general, coupling can be caused by inertial coupling effects, aerodynamic coupling, or engine gyroscopic effects. Although the relative magnitude of each type of coupling has not been determined for the X-5 airplane, examination of the time histories would indicate that both gyroscopic and aerodynamic coupling are present in appreciable amounts.

Figures 3(b) and 3(c) show the coupling from longitudinal to lateral directional mode for an elevator pulse. Note that an up-elevator pulse produces a right yawing motion, whereas a down-elevator pulse produces a left yaw. Since the aerodynamic coupling to the lateral mode from a disturbance in pitch is usually negligible, this coupling is believed due to gyroscopic effects. The initial directions of coupled motion for the two disturbance directions agree with those expected from the gyroscopic precessional torque of the jet engine.

Figures 6(a) and 6(b) show the coupling from the lateral mode to the longitudinal mode for rudder pulses. These time histories show that a right rudder pulse produces a small initial decrease in angle of attack and a left rudder pulse produces a large increase in angle of attack. Again gyroscopic coupling is implied; however, there are large initial amplitude and phase differences in the coupled oscillation for right and left rudder pulses, suggesting the probability of both aerodynamic and gyroscopic coupling. Sideslips performed with the airplane have shown no appreciable pitching moments caused by sideslip, indicating no static aerodynamic coupling.

In the X-5 airplane configuration the mass is concentrated to a large extent in the fuselage and near the center of gravity. This physical characteristic makes the moments of inertia about the Y- and Z-axes relatively small as compared with a conventional jet-powered airplane of comparable weight (determined experimentally by the method of ref. 6, $I_Y = 9,495 \text{ slug-ft}^2$, $I_Z = 10,110 \text{ slug-ft}^2$). Therefore, engine gyroscopic torques are effective in producing disturbances in pitch and yaw. It will also be noted by comparing figure 4 and figure 9 that the periods of the longitudinal and lateral oscillations are almost equal. This condition will produce a near resonant state for the gyroscopic coupling

torque and resultant coupled oscillation. In this case a poorly damped oscillation in either the longitudinal or lateral mode would produce a forced resonant oscillation in the other mode. For example, an elevator pulse in the directional nonlinear damping region would couple a disturbance to the lateral mode, producing a small poorly damped oscillation which is coupled back to the longitudinal mode and appears there as a near resonant forced oscillation. For these reasons engine gyroscopic effects are considered important in an analysis of the characteristics of the X-5 airplane.

Frequency Response

The transient responses of the X-5 airplane have been analyzed by means of the Fourier transform and the frequency response obtained. These calculations were made in order to present the dynamic characteristics of the airplane in a form that would be more usable to automatic control system designers. The calculations were made on an IBM machine calculator by a numerical integration procedure using the methods of reference 7. The data selected for analysis were from the same transient responses previously discussed and were analyzed about the airplane body axis. In addition to the above transients, a series of aileron pulses were made over the Mach number range for frequency response only. The airplane responses analyzed and presented in this paper are $\dot{\theta}/\delta_e$, β/δ_r , $\dot{\psi}/\delta_r$, $\dot{\theta}/\delta_r$, $\dot{\phi}/\delta_r$, and $\dot{\phi}/\delta_a$.

Reference 8 shows that the frequency-response characteristics are invariant with control pulse shape and size only when the system is linear. It has been shown previously that the lateral mode of the X-5 airplane is nonlinear in damping over part of the amplitude range of the oscillation. The frequency-response curves therefore represent the airplane only for the range of rudder amplitudes used in this investigation.

Presented in figure 14(a) are typical results of the investigation in the longitudinal mode, showing the frequency response of the pitching velocity for an elevator input $\dot{\theta}/\delta_e$ as obtained by analyzing an elevator pulse maneuver. This figure shows the amount of scatter obtained in the calculated response points and the fairing made in such cases. Figures 14(b) to 14(d) present composites of these curves showing the Mach number variation. The double peak found in these responses is rather unusual and at first seems to indicate the presence of two modes of oscillation with natural frequencies fairly close together. The similarity in magnitude of the natural frequencies of the longitudinal and directional modes plus the large mode coupling appears to offer a basis for explanation of the shape of the longitudinal frequency-response curves. However, the time histories of pitching velocity do not appear

to contain two frequency modes, nor is there any natural frequency in pitch or yaw closely corresponding to the lower frequency-response peak. In an effort to show the effects of engine gyroscopic coupling, tests were made performing elevator pulses at a given speed and altitude with the engine idling and at maximum revolutions per minute. To achieve as large a difference in engine speed as possible, the tests were performed at 15,000 feet where the engine can be idled as low as 60 percent of maximum rpm. The tests consisted of a pulse made with the engine idling at 60 percent of maximum rpm while the airplane speed was decreasing through $M = 0.6$. Another pulse at 100 percent rpm was made while the airplane speed was increasing through $M = 0.6$. The frequency-response calculations for these pulses are presented in figure 15. The frequency-response plot shows that the difference between the maximum and minimum in the double peak is slightly less for the low rpm than for the 100 percent case. This difference would tend to substantiate the fact that there is an engine gyroscopic moment acting on the airplane. However, considering the accuracy of the tests, the differences are too small for any definite conclusions to be drawn.

In a further attempt to determine the cause of the double peak longitudinal frequency response, calculations of longitudinal frequency response were made from theoretical transfer functions derived from simplified equations of motion as shown in the appendix. Two sets of calculations were made, assuming first a two-degree-of-freedom system and then a three-degree-of-freedom system. The two-degree-of-freedom system consisted of the classical longitudinal equations and assumed constant forward velocity. The three-degree-of-freedom system included the same two previous equations, modified to include a moment term due to gyroscopic coupling from yawing velocity. The third degree of freedom was assumed to be yaw about the Z-axis. This equation also included a moment term due to gyroscopic coupling from pitching velocity. The transfer function θ/δ_e was obtained for both the two- and three-degree-of-freedom cases and the frequency response was calculated by using longitudinal and simplified lateral derivatives which were obtained by assuming only a single degree of lateral freedom. These lateral derivatives were calculated from the flight data as described in the appendix. These theoretical frequency-response calculations were made for two Mach numbers, $M = 0.70$ and $M = 0.87$, at 40,000 feet and are presented in figures 16(a) and 16(b). The responses are admittedly rough approximations to the actual airplane frequency responses, since at least two degrees of lateral freedom are neglected along with all inertial and aerodynamic coupling terms. However, it is evident that the dominant airplane response characteristics are demonstrated by the simplified three-degree-of-freedom calculations. Figure 16(b) shows that the frequency responses obtained from the transfer function of the three-degree-of-freedom system match in general shape and amplitude the frequency responses obtained experimentally (fig. 14). The agreement of frequency location for the corresponding peaks in these figures is not too good.

Results of calculations of $\dot{\theta}/\delta_e$ for the classical two-degree-of-freedom system, neglecting coupling, are given in figure 16(a). It is interesting to note, in comparing the two-degree-of-freedom system to the three-degree-of-freedom system, that the frequency locations of all the peaks differ. The transfer functions were factored to determine the roots of the numerator and denominator. The classical two-degree-of-freedom system was found to be of the form

$$\frac{\dot{\theta}}{\delta_e} = \frac{(D + \gamma)}{(D^2 + AD + B)}$$

where the denominator has a pair of conjugate complex roots. The three-degree-of-freedom system transfer function was found to have the form

$$\frac{\dot{\theta}}{\delta_e} = \frac{(D + \gamma_1)(D^2 + A_1D + B_1)}{(D^2 + A_2D + B_2)(D^2 + A_3D + B_3)}$$

with a real root and a pair of conjugate complex roots in the numerator and two pairs of conjugate complex roots in the denominator. The complex roots indicate that this system has two natural frequencies. However, as shown by the values of the roots given in the appendix, the conjugate complex pair in the numerator is close to the value of one of the conjugate complex pairs in the denominator and tends to cancel the effects of the latter.

Figures 17, 18, 19, and 20 present, respectively, the results of the experimental frequency-response calculations for rudder pulse β/δ_r , $\dot{\psi}/\delta_r$, $\dot{\phi}/\delta_r$, and $\dot{\theta}/\delta_r$. Since some differences were noted on the time histories between the airplane response to right and left pulses, the frequency-response characteristics are presented separately for right and left pulses. Also presented in each figure is a plot showing the individual calculated points for a specific type of response. Plots of β/δ_r are presented in figures 17(a) to 17(c). It will be noticed that the frequency-response variations with Mach number are not always consistent. It is not known whether this lack of consistency is due to nonlinearity in some aerodynamic parameters or to scatter in the data. The composites for right and left rudder pulses show little difference except that the left pulses have a smaller amplitude ratio peak at the lowest Mach numbers. The general remarks made about β/δ_r are true also for $\dot{\psi}/\delta_r$ and $\dot{\phi}/\delta_r$ (figs. 18 and 19). However, for the rolling velocity response $\dot{\phi}/\delta_r$ (fig. 19) the right pulse amplitude ratio peaks appear to increase somewhat over the left at the highest Mach numbers. The pitching response to rudder disturbance $\dot{\theta}/\delta_r$ is presented in

figure 20. Although the differences in amplitude ratio are small for right and left pulses, the differences in phase angle are large. These differences were noted previously from an examination of time histories.

Aileron pulses in both directions were also made and responses were analyzed in frequency response form. The results for rolling velocity response $\dot{\phi}/\delta_a$ are presented in figure 21. Again, large differences are noted in the curves for right and left pulse groups. An effort was made to obtain the frequency response $\dot{\psi}/\delta_a$ but the results were not of sufficient quality to present.

Because of the complicated nature of the transfer functions of this airplane and the presence of some nonlinear derivatives, no attempt has been made to determine the lateral stability derivatives, except some simplified derivatives for the longitudinal frequency-response calculation described in the appendix.

CONCLUDING REMARKS

An investigation of the dynamic stability of the X-5 research airplane at 58.7° sweepback at altitudes of 40,000 feet and 25,000 feet over a Mach number range of 0.50 to 0.97 shows the following: The longitudinal motions are well damped over the entire Mach number range tested except for residual oscillations resulting principally from engine gyroscopic coupling with the lateral oscillatory mode. This engine gyroscopic coupling results in motion in both the longitudinal and lateral oscillatory modes for either a longitudinal or lateral disturbance. The lateral oscillatory mode exhibits moderately good damping except for nonlinear damping characteristics above a Mach number of 0.80 where the motion is well damped at large amplitudes and poorly damped for double amplitude sideslip angles smaller than 2° . Small inadvertent aileron control motions often produce apparently undamped small amplitude oscillations in the Mach number range above 0.80.

By the current military aircraft dynamic stability requirements, the lateral oscillation is unsatisfactory over most of the Mach number range. The pilots concur with this finding and report the airplane to be particularly intolerable in the range with nonlinear damping characteristics.

The longitudinal frequency response $\dot{\theta}/\delta_e$ has a large and unusual double peak near the short period natural frequency. Theoretical calculations have shown that engine gyroscopic coupling effects are principally responsible for the shape of the $\dot{\theta}/\delta_e$ frequency-response curves.

Lateral frequency-response calculations show some differences for right and left rudder or aileron pulse disturbances, particularly the longitudinal response to a rudder pulse $\dot{\theta}/\delta_r$ and the lateral response to an aileron pulse $\dot{\phi}/\delta_a$.

High-Speed Flight Station,
National Advisory Committee for Aeronautics,
Edwards, Calif., August 3, 1955.

APPENDIX

DERIVATION OF A SIMPLIFIED THEORETICAL TRANSFER FUNCTION
DESCRIBING THE ENGINE GYROSCOPIC COUPLING EFFECTS

The form of the equations of the two-degree-of-freedom system and its transfer function will not be presented in this paper since it is generally well known and may be found in reference 6. All the derivatives and airplane constants used in the calculations are contained in the derivatives and constants listed for the three-degree-of-freedom system (table II).

The equations of motion assumed for the three-degree-of-freedom system are:

$$\frac{mV}{qS} D(\theta - \alpha) = C_{L\alpha}\alpha + C_{L\delta_e}\delta_e \quad (1)$$

$$\frac{I_Y}{qS\bar{c}} D^2\theta = C_{m\alpha}\alpha + \bar{C}_{m\dot{\alpha}}D\alpha + \bar{C}_{m\dot{\theta}}D\theta + C_{m\dot{\psi}}D\psi + C_{m\delta_e}\delta_e \quad (2)$$

$$\frac{I_Z}{qSb} D^2\psi = C_{n\psi}\psi + C_{n\dot{\psi}}D\psi + C_{n\dot{\theta}}D\theta \quad (3)$$

These equations assume that the stability axes coincide with the airplane principal axes of inertia and that there are two-degrees-of-longitudinal freedom and one-degree-of-lateral freedom. In formulating these equations it was assumed that the rotating engine mass produced gyroscopic moment proportional to the precessional angular velocity where

R = axial moment of inertia, slug-ft²

G = spin of engine mass, radians/sec

A = precessional angular velocity, radians/sec

Q = moment, ft-lb

The coupling derivatives $C_{m\dot{\psi}}$ and $C_{n\dot{\theta}}$ were obtained as follows: Let

M = pitching moment

CONFIDENTIAL

then

$$C_m = \frac{M}{qS\bar{c}}$$

letting

$$M = Q = RGA$$

$$C_m = \frac{RGA}{qS\bar{c}}$$

$$C_{m\dot{\psi}} = \frac{dC_m}{d(\dot{\psi})} = \frac{RG}{qS\bar{c}}$$

where

$$A = \dot{\psi}$$

The yawing-moment derivative $C_{n\dot{\theta}}$ is obtained in a similar manner so that $C_{n\dot{\theta}} = \frac{RG}{qSb}$. The derivative $C_{n\dot{\psi}}$ corresponds to the usual derivative $C_{n\beta}$. In assuming a single-degree-of-lateral freedom $-\beta = \psi$ and $-C_{n\beta} = C_{n\dot{\psi}}$. For this simplified case

$$C_{n\dot{\psi}} = \frac{-I_Z}{qSb} \left[\left(\frac{2\pi}{P} \right)^2 + \left(\frac{0.693}{T_{1/2}} \right)^2 \right]$$

This relationship was used to calculate $C_{n\dot{\psi}}$. The other lateral derivative $C_{n\dot{\psi}}$ was found to have a very small effect and was estimated. The other derivatives in table II were obtained from figures and references presented in this paper. In solving the equation, let

$$\frac{mV}{qS} = k_1$$

$$\frac{I_Y}{qS\bar{c}} = k_2$$

$$\frac{I_Z}{qSb} = k_3$$

Divide both sides of equation (1) by k_1 , equation (2) by k_2 , and equation (3) by k_3 . By solving these equations $\dot{\theta}/\delta_e$ is obtained as

$$\frac{\dot{\theta}}{\delta_e} = \frac{A_1 D^3 + A_2 D^2 + A_3 D + A_4}{D^4 + A_5 D^3 + A_6 D^2 + A_7 D + A_8}$$

here

$$A_1 = \frac{C_{m\delta_e}}{k_2} + \frac{C_{m\dot{\alpha}} C_{L\delta_e}}{k_1 k_2}$$

$$A_2 = \left[\frac{C_{m\alpha}}{k_1 k_2} - \frac{C_{n\psi} C_{m\dot{\alpha}}}{k_1 k_2 k_3} \right] C_{L\delta_e} + \left[\frac{C_{L\alpha}}{k_1 k_2} - \frac{C_{n\psi}}{k_2 k_3} \right] C_{m\delta_e}$$

$$A_3 = - \frac{(C_{n\psi} C_{m\dot{\alpha}} + C_{n\dot{\psi}} C_{m\alpha}) C_{L\delta_e}}{k_1 k_2 k_3} + \left(\frac{C_{n\psi}}{k_2 k_3} + C_{n\dot{\psi}} C_{L\alpha} \right) C_{m\delta_e}$$

$$A_4 = - \left[C_{m\alpha} C_{n\psi} C_{L\delta_e} + C_{n\psi} C_{L\alpha} C_{m\delta_e} \right] \frac{1}{k_1 k_2 k_3}$$

$$A_5 = - \left[\frac{C_{m\dot{\theta}} + C_{m\dot{\alpha}}}{k_2} - \frac{C_{L\alpha}}{k_1} + \frac{C_{n\dot{\psi}}}{k_3} \right]$$

$$A_6 = - \frac{C_{L\alpha} C_{m\dot{\theta}}}{k_1 k_2} + \frac{C_{n\dot{\psi}}}{k_2 k_3} (C_{m\dot{\theta}} + C_{m\dot{\alpha}}) - \frac{C_{n\dot{\psi}} C_{L\alpha}}{k_1 k_2 k_3} - \frac{C_{n\dot{\psi}}}{k_3} - \frac{C_{m\dot{\psi}} C_{n\dot{\theta}}}{k_2 k_3} - \frac{C_{m\alpha}}{k_2}$$

$$A_7 = \frac{C_{n\dot{\psi}} (C_{m\dot{\theta}} + C_{m\dot{\alpha}})}{k_2 k_3} + \frac{C_{L\alpha} (C_{n\dot{\psi}} C_{m\dot{\theta}} - k_2 C_{n\dot{\psi}} - C_{m\dot{\psi}} C_{n\dot{\theta}})}{k_1 k_2 k_3} + \frac{C_{n\dot{\psi}} C_{m\alpha}}{k_2 k_3}$$

$$A_8 = \frac{C_{n\dot{\psi}} C_{L\alpha} C_{m\dot{\theta}}}{k_1 k_2 k_3} + \frac{C_{m\alpha} C_{n\dot{\psi}}}{k_2 k_3}$$

The frequency response was obtained from this transfer function by substituting into the transfer function the proper values of the constants and $D = i\omega$.

Substituting the aerodynamic coefficients at $M = 0.87$ into the transfer functions and factoring yields the following expressions: Two degrees of freedom

$$\frac{-15.082D + 1.510}{D^2 + 2.8520D + 19.3572}$$

Three degrees of freedom

$$\frac{15.082D^3 - 8.817D^2 - 195.082D - 19.451}{D^4 + 3.337D^3 + 35.567D^2 + 47.009D + 249.446}$$

or

$$\frac{15.082(D + 0.0999)(D^2 + 0.483D + 12.886)}{(D^2 + 2.56D + 21.8)(D^2 + 0.80D + 11.3)}$$

REFERENCES

1. Bellman, Donald R.: Lift and Drag Characteristics of the Bell X-5 Research Airplane at 59° Sweepback for Mach Numbers From 0.60 to 1.03. NACA RM L53A09c, 1953.
2. Finch, Thomas W.: Flight Determination of the Longitudinal Stability and Control Characteristics of the Bell X-5 Research Airplane at 58.7° Sweepback. NACA RM H55C07, 1955.
3. Finch, Thomas W., and Walker, Joseph A.: Flight Determination of the Static Longitudinal Stability Boundaries of the Bell X-5 Research Airplane With 59° Sweepback. NACA RM L53A09b, 1953.
4. Anon.: Military Specification - Flying Qualities of Piloted Airplanes. MIL-F-8785 (ASG), 1 September 1954.
5. Anon.: Flying Qualities of Piloted Airplane. U. S. Air Force Specification No. 1815-B, June 1, 1948.
6. Turner, Howard L.: Measurement of the Moments of Inertia of an Airplane by a Simplified Method. NACA TN 2201, 1950.
7. Schumacher, Lloyd E.: Methods for Analyzing Transient Flight Data to Obtain Aircraft Frequency Response. AF, Air Materiel Command, Wright-Patterson A.F.B. (Flight Test Div. Memo. Rep.) Ser. MCRFT-2268, Jan. 1950.
8. Triplett, William C., and Smith, G. Allan: Longitudinal Frequency-Response Characteristics of a 35° Swept-Wing Airplane as Determined From Flight Measurements, Including a Method for the Evaluation of Transfer Functions. NACA RM A51G27, 1951.

TABLE I

PHYSICAL CHARACTERISTICS OF BELL X-5 AIRPLANE AT A SWEEP ANGLE OF 58.7°

Airplane:

Weight, lb:	
Full fuel	10,006
Less fuel	7,894
Power plant:	
Axial-flow turbojet engine	J35-A-17
Center-of-gravity position, percent M.A.C.:	
Full fuel	45.0
Less fuel	45.5
Moments of inertia for 58.7° sweep (clean configuration full fuel,	
body axis), slug-ft ² :	
About X-axis	5,165
About Y-axis	9,495
About Z-axis	10,110
Overall height, ft	12.2
Overall length, ft	33.6

Wing:

Airfoil section (perpendicular to 38.02-percent-chord line):	
Root	NACA 64(10)A011
Tip	NACA 64(08)A008.28
Sweep angle at 0.25 chord, deg	58.7
Area, sq ft	183.7
Span, ft	20.1
Span between equivalent tips, ft	19.3
Aspect ratio	2.20
Taper ratio	0.411
Mean aerodynamic chord, ft	9.95
Location of leading edge of mean aerodynamic chord, fuselage station	101.2
Incidence root chord, deg	0
Dihedral, deg	0
Geometric twist, deg	0
Wing flaps (split):	
Area, sq ft	15.9
Span, parallel to hinge center line, ft	6.53
Chord, parallel to line of symmetry at 20° sweepback, in.:	
Root	30.8
Tip	19.2
Travel, deg	60
Slats (leading edge divided):	
Area, sq ft	14.6
Span, parallel to leading edge, ft	10.3
Chord, perpendicular to leading edge, in.:	
Root	11.1
Tip	6.6
Travel, percent wing chord:	
Forward	10
Down	5
Aileron (45 percent internal-seal pressure balance):	
Area (each aileron behind hinge line), sq ft	3.62
Span parallel to hinge center line, ft	5.15
Travel, deg	±15
Chord, percent wing chord	19.7
Moment area rearward of hinge line (total), in. ³	4,380

TABLE I.- Concluded

PHYSICAL CHARACTERISTICS OF BELL X-5 AIRPLANE AT A SWEEP ANGLE OF 58.7°

Horizontal tail:

Airfoil section (parallel to fuselage center line) . . .	NACA 65A006
Area, sq ft	31.5
Span, ft	9.56
Aspect ratio	2.9
Taper ratio	0.371
Sweep angle at 0.25-percent chord, deg	45
Mean aerodynamic chord, in.	42.8
Position of 0.25 mean aerodynamic chord, fuselage station . .	355.6
Stabilizer travel, (power actuated), deg:	
Leading edge up	4.5
Leading edge down	7.5
Elevator (20.8 percent overhang balance, 31.5 percent span):	
Area rearward of hinge line, sq ft	6.9
Travel from stabilizer, deg:	
Up	25
Down	20
Chord, percent horizontal tail chord	30
Moment area rearward of hinge line (total), in. ³	4,200

Vertical tail:

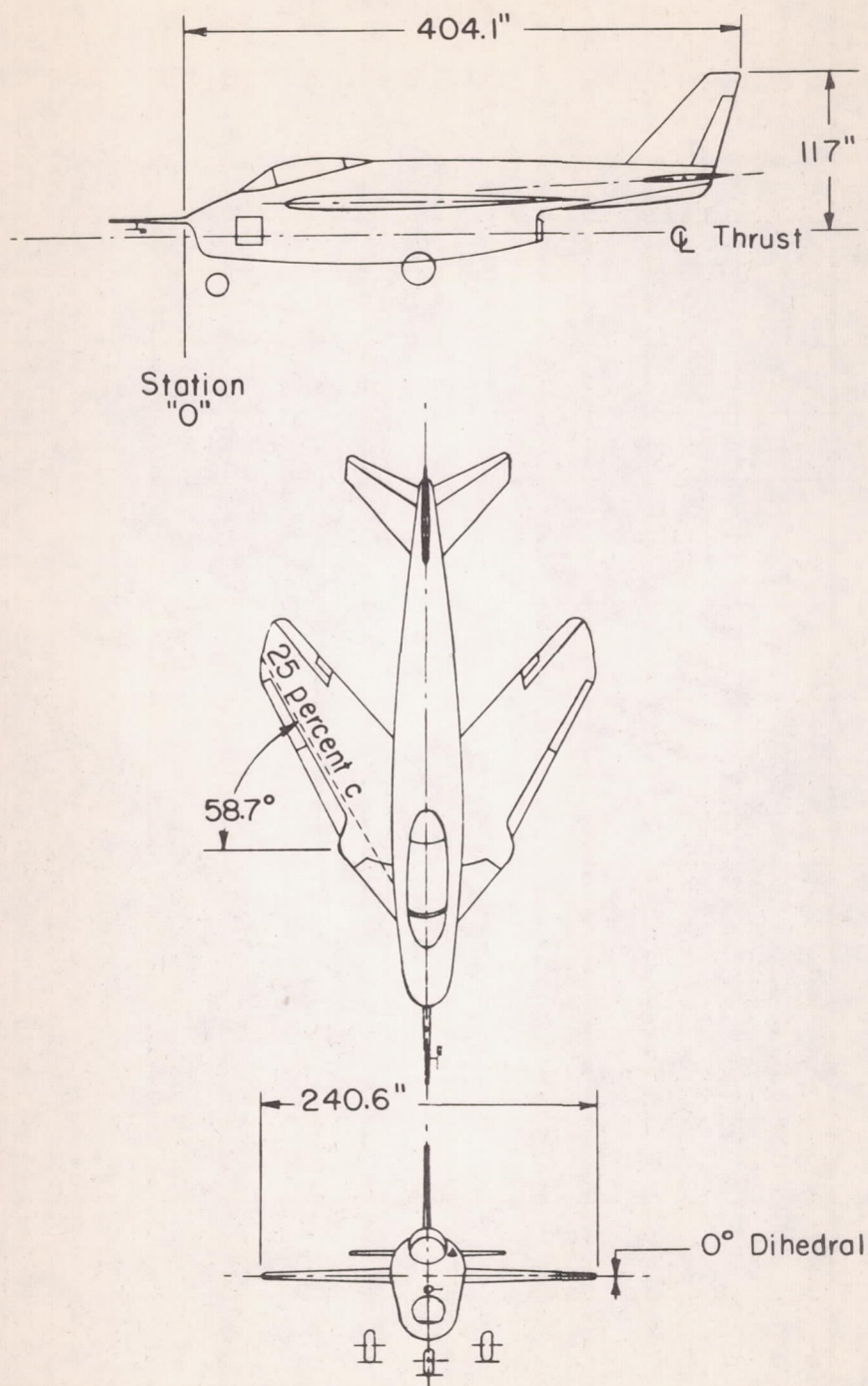
Airfoil section (parallel to rear fuselage center line)	NACA 65A006
Area, (above rear fuselage center line), sq ft	25.8
Span, perpendicular to rear fuselage center line, ft	6.17
Aspect ratio	1.47
Sweep angle of leading edge, deg	46.6
Fin:	
Area, sq ft	24.8
Rudder (23.1 percent overhang balance, 26.3 percent span):	
Area rearward of hinge line, sq ft	4.7
Span, ft	4.43
Travel, deg	±35
Chord, percent horizontal tail chord	22.7
Moment area rearward of hinge line, in. ³	3,585

TABLE II

PARAMETERS USED IN ESTIMATING AIRPLANE FREQUENCY RESPONSE

$$[h_p = 40,000 \text{ feet}]$$

	M	0.70	0.87
V, fps		680	845
q, lb/sq ft		133	199
S, sq ft		183.7	183.7
\bar{c} , ft		9.95	9.95
b, ft		20.1	20.1
$C_{L\alpha}$, radian ⁻¹		2.80	2.865
$C_{L\delta}$, radian ⁻¹		-1.976	-1.848
$C_{m\alpha}$, radian ⁻¹		-.4870	-.4854
$\bar{C}_{m\dot{\alpha}}$, (radians/sec) ⁻¹		-.0070	-.0070
$C_{m\delta}$, radian ⁻¹		-.3438	-.3780
$\bar{C}_{m\dot{\theta}} + \bar{C}_{m\dot{\alpha}}$, (radians/sec) ⁻¹		-.0592	-.0597
$\bar{C}_{m\dot{\theta}}$, (radians/sec) ⁻¹		-.0522	-.0527
$C_{m\dot{\psi}}$, (radians/sec) ⁻¹		-.0556	-.0372
$C_{n\dot{\theta}}$, (radian/sec) ⁻¹		.0278	-.0187
$C_{n\psi}$, radian ⁻¹		-.2350	-.1862
$C_{n\dot{\psi}}$, (radians/sec) ⁻¹		-.0100	-.007



(a) Three-view drawing.

Figure 1.- Bell X-5 research airplane at 58.7° sweepback.



(b) Photograph.

L-87906

Figure 1.- Concluded.

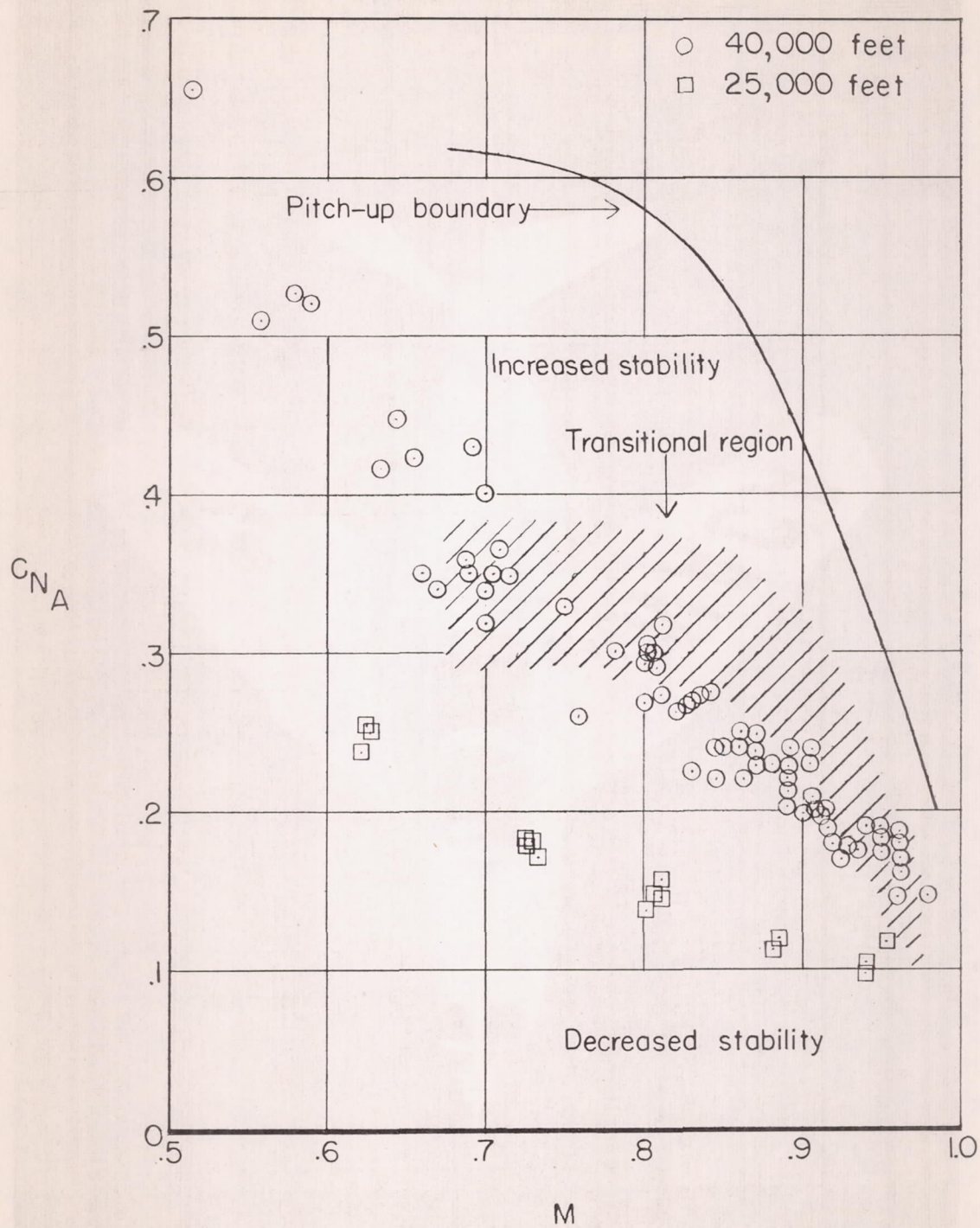
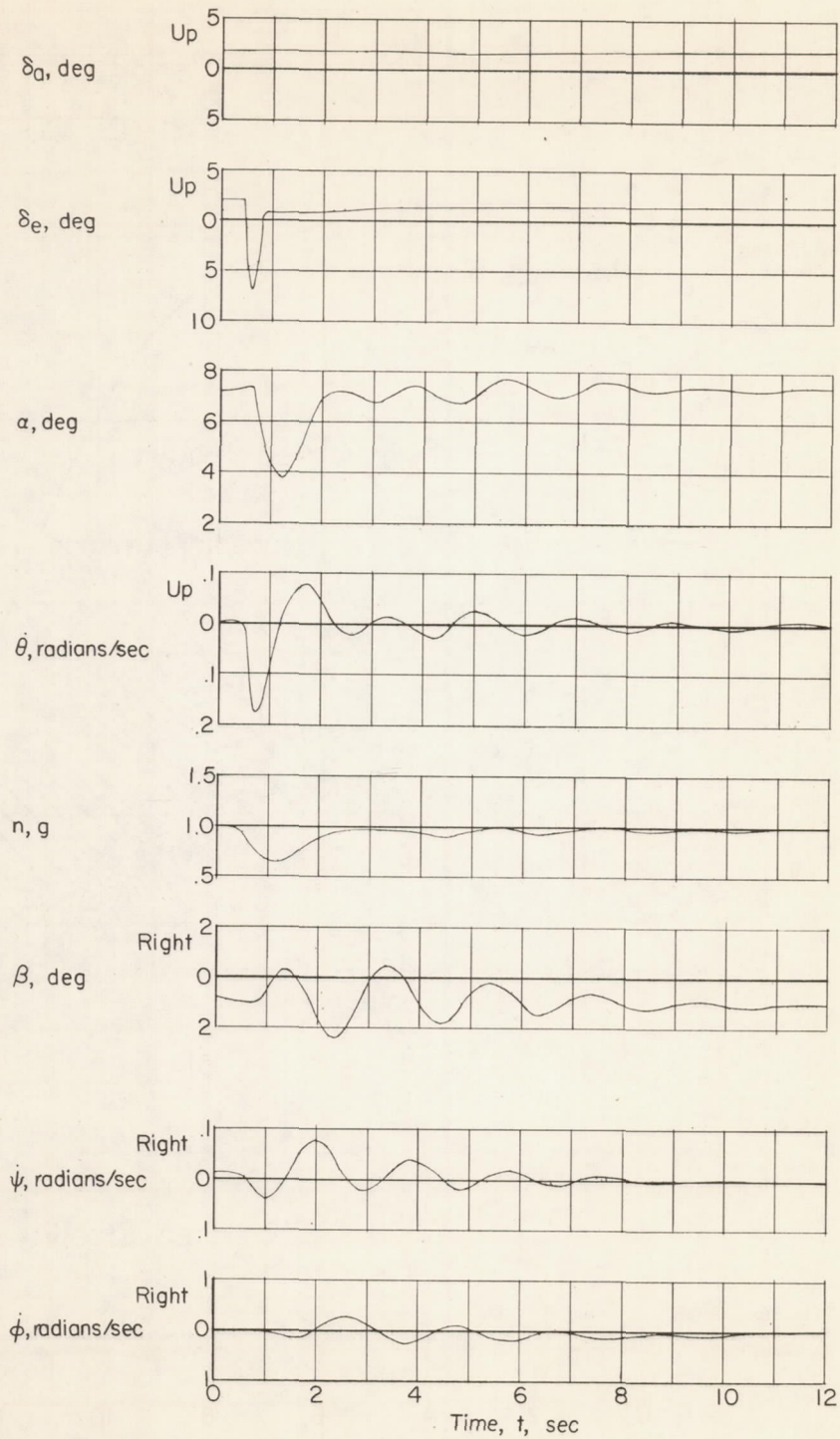
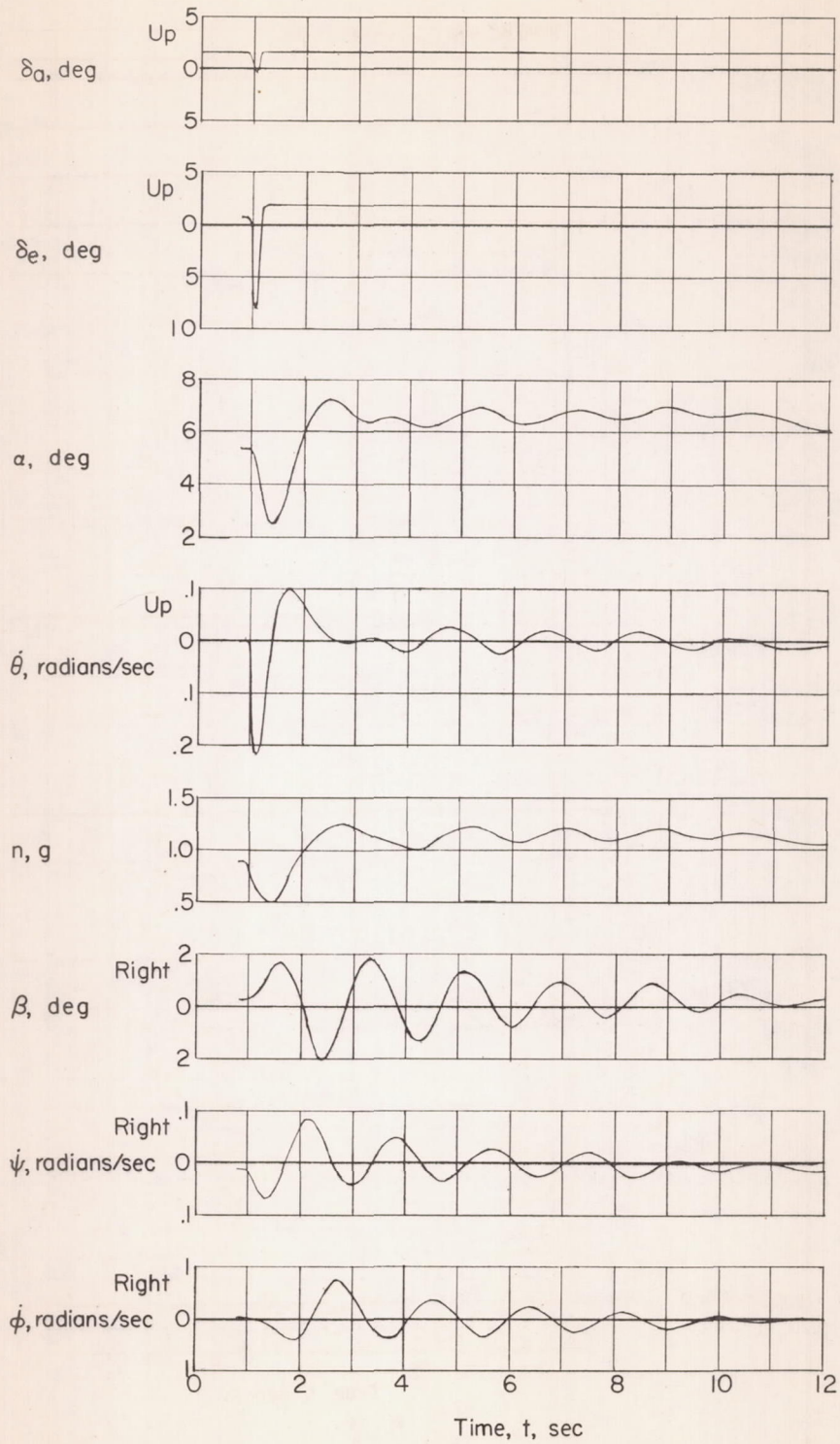


Figure 2.- Average C_{NA} during pulse maneuver.



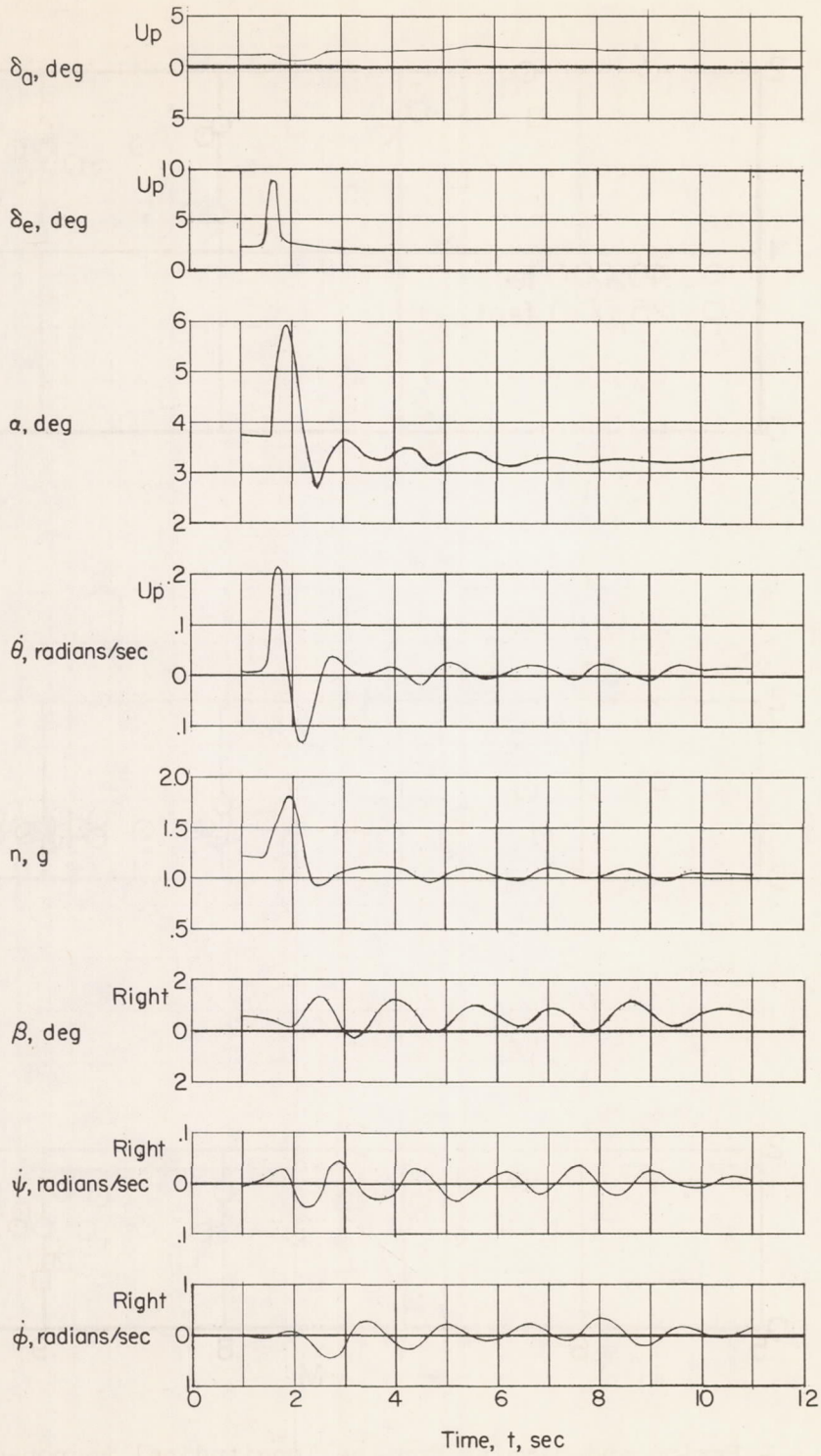
(a) $M = 0.70$.

Figure 3.- Time history of airplane transient oscillation in response to elevator pulse at 40,000 feet.



(b) $M = 0.85$.

Figure 3.- Continued.



(c) $M = 0.96$.

Figure 3.- Concluded.

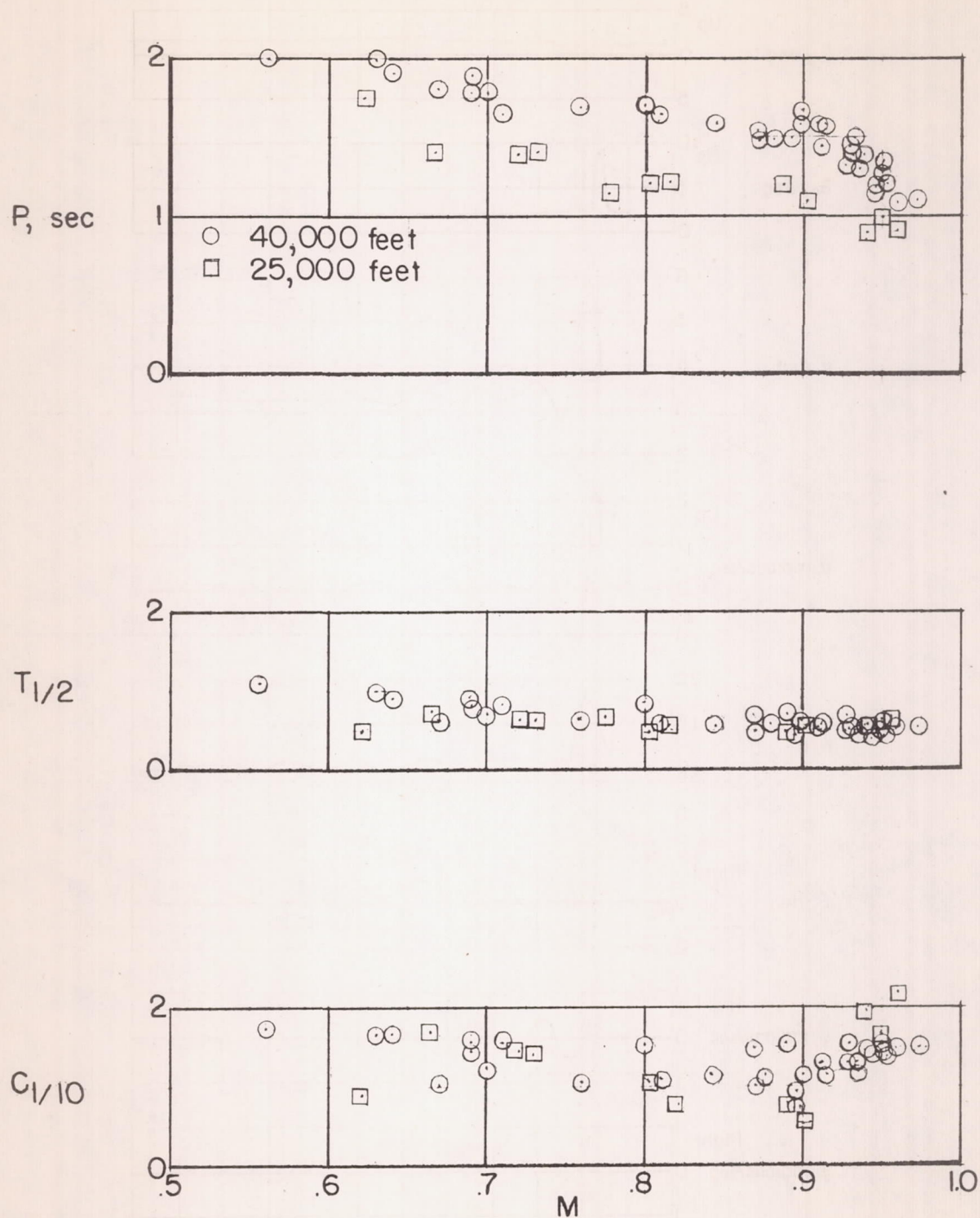


Figure 4.- Period and damping for the longitudinal response of the X-5 airplane to an elevator pulse.

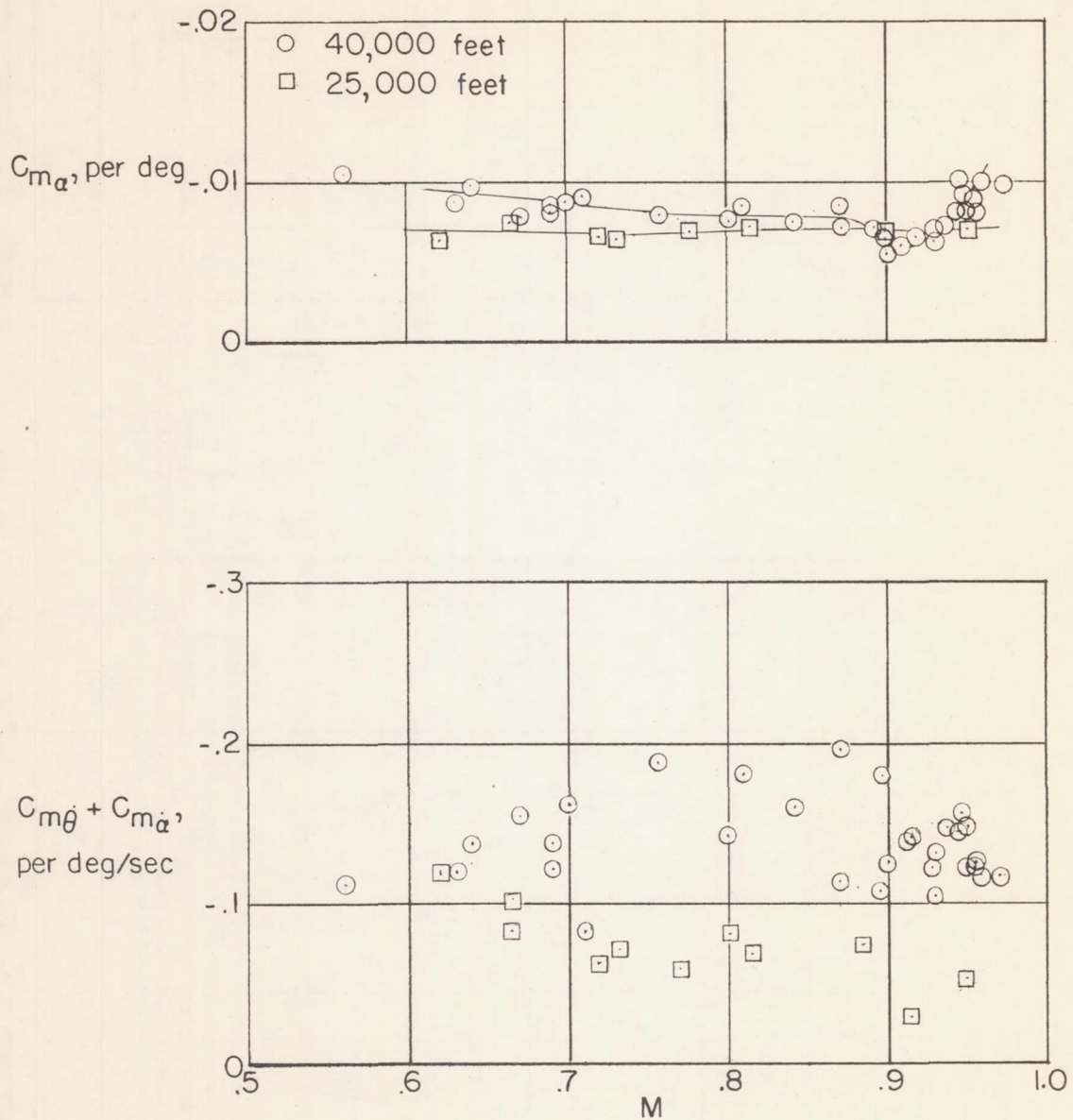


Figure 5.- Variation of the longitudinal stability derivatives $C_{m\alpha}$ and $C_{m\dot{\theta}} + C_{m\dot{\alpha}}$ with Mach number.

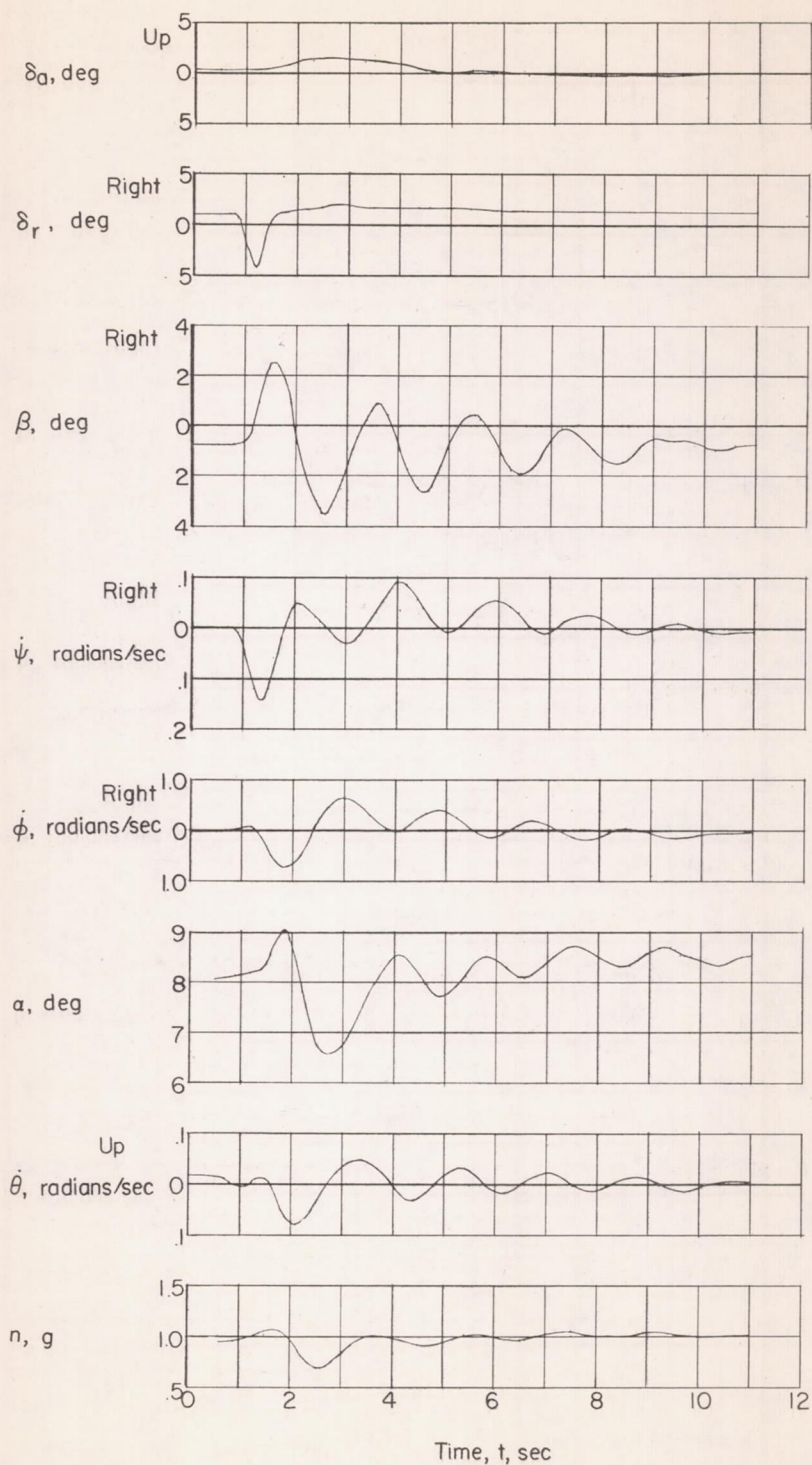
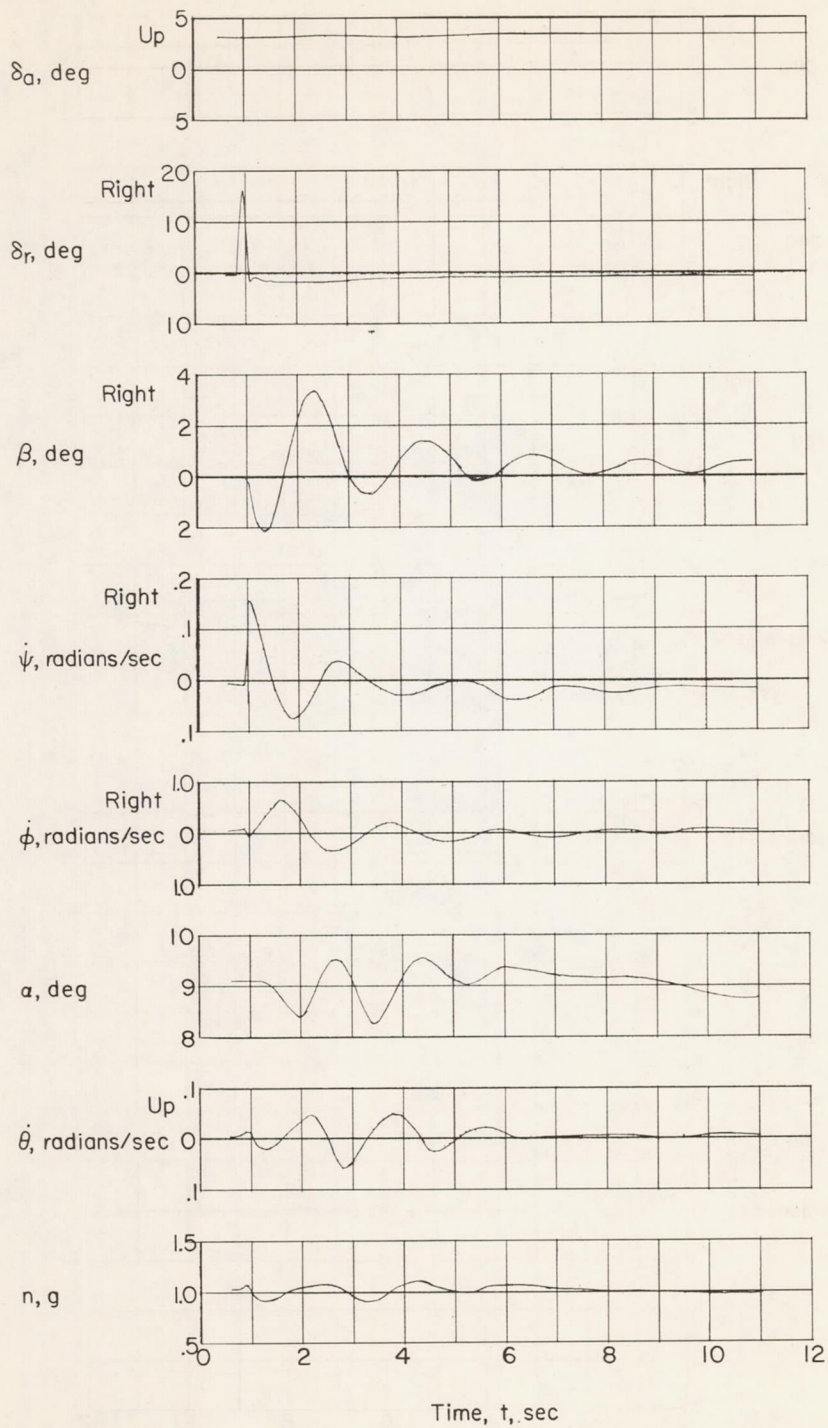
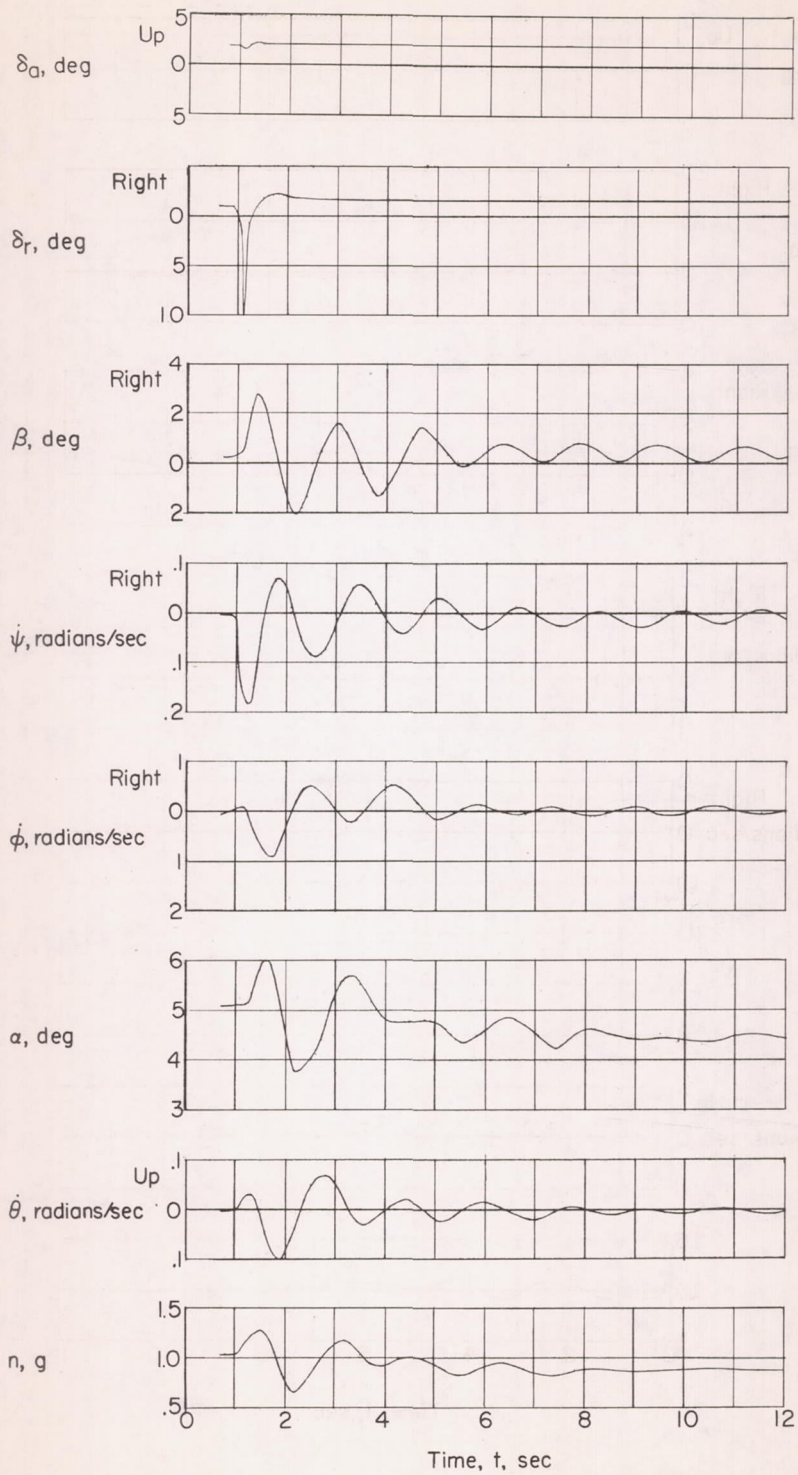
(a) $M = 0.70$.

Figure 6.- Time histories of transient oscillations in response to a rudder pulse at 40,000 feet.



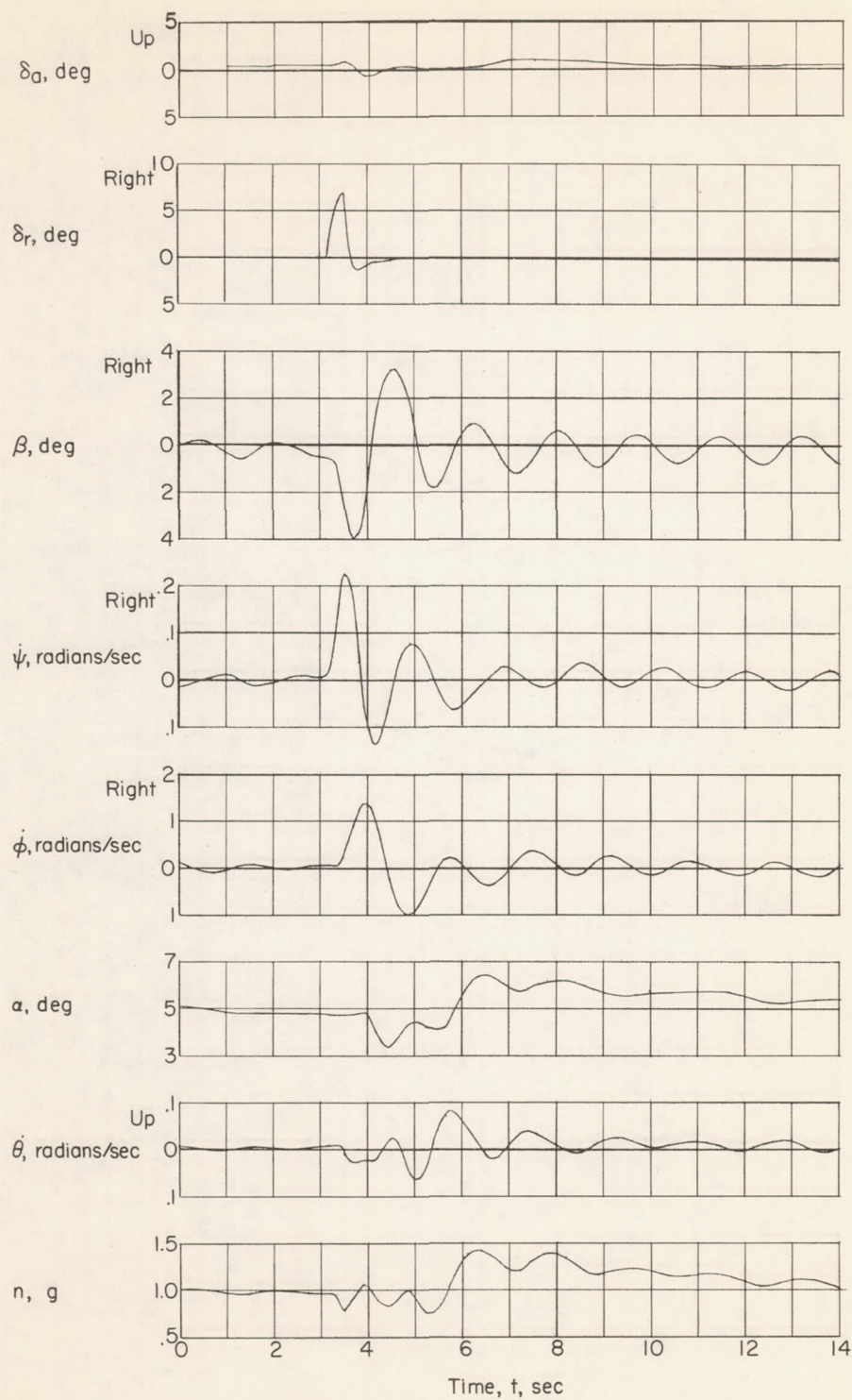
(b) $M = 0.67$.

Figure 6.- Continued.



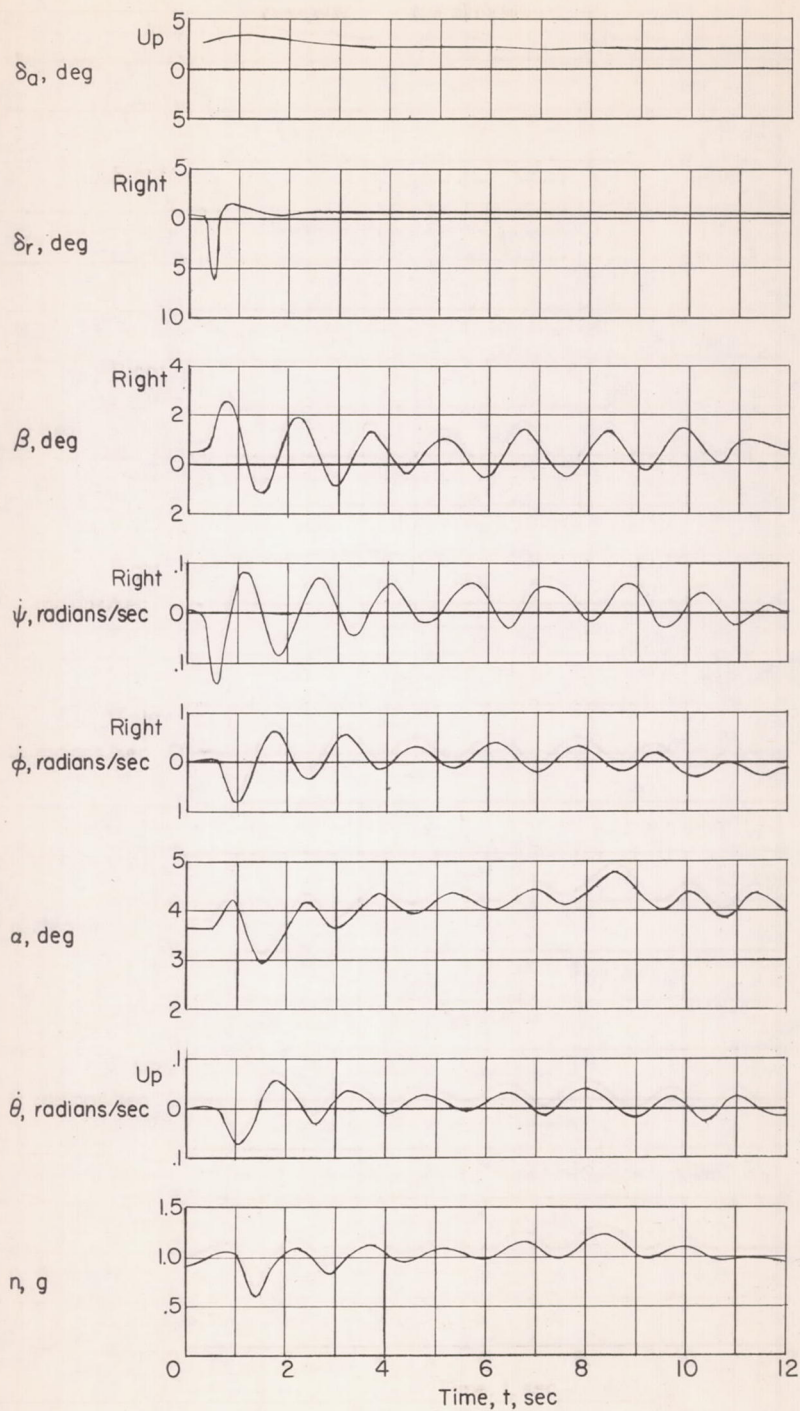
(c) $M = 0.89$.

Figure 6.- Continued.



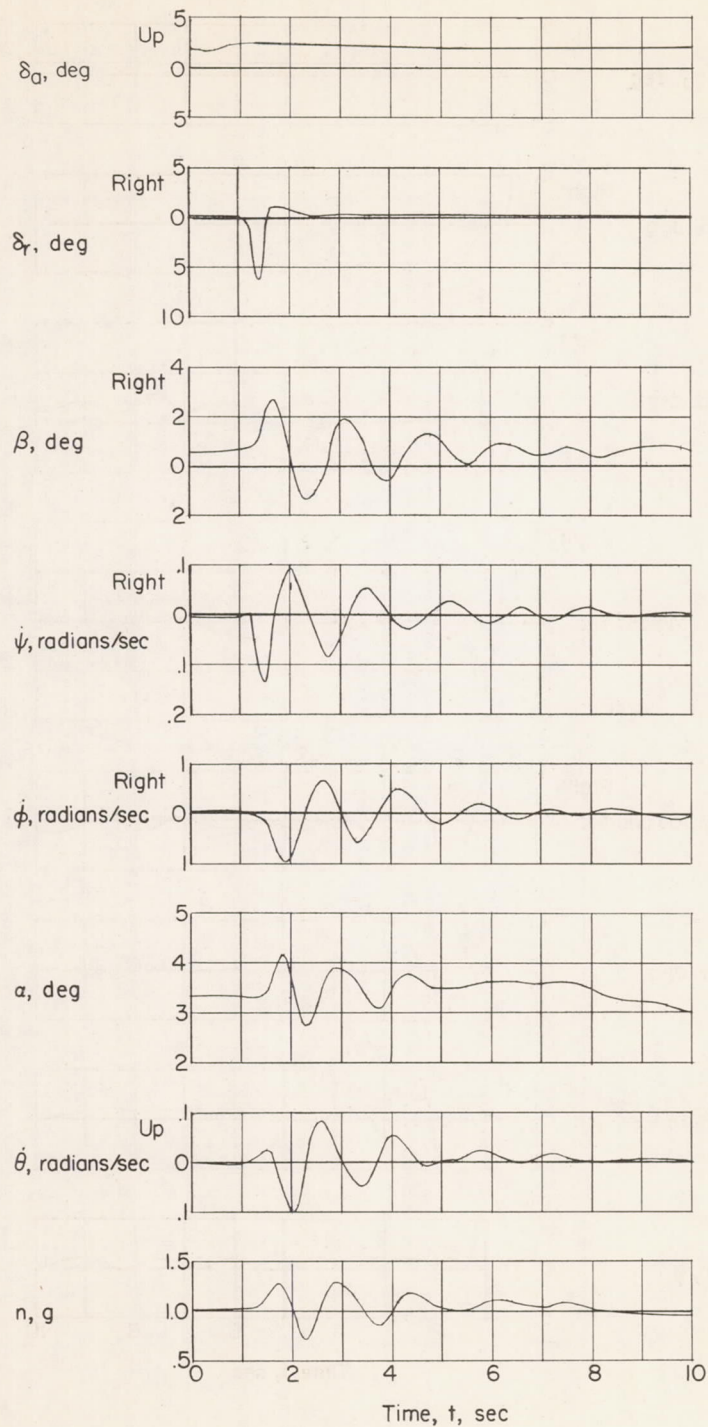
(d) $M = 0.89$.

Figure 6.- Continued.



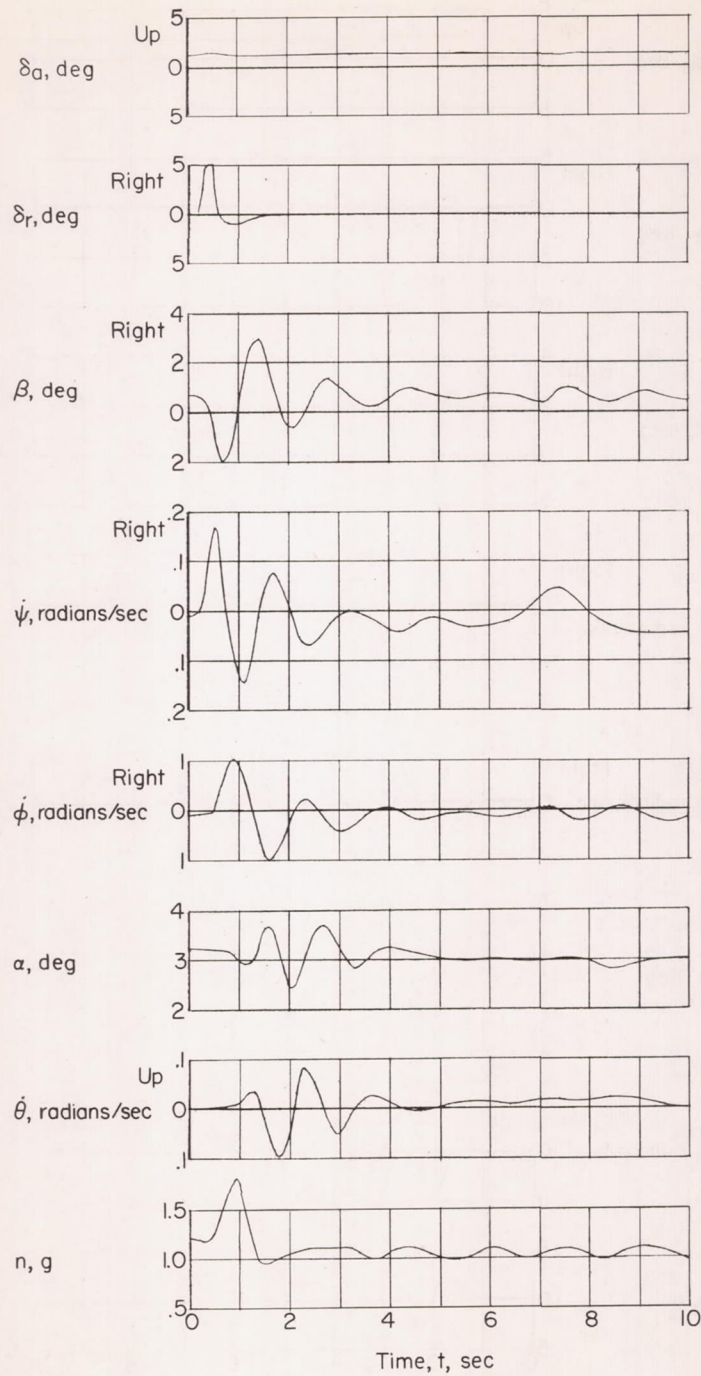
(e) $M = 0.94$.

Figure 6.- Continued.



(f) $M = 0.96$.

Figure 6.- Continued.



(g) $M = 0.96$.

Figure 6.- Concluded.

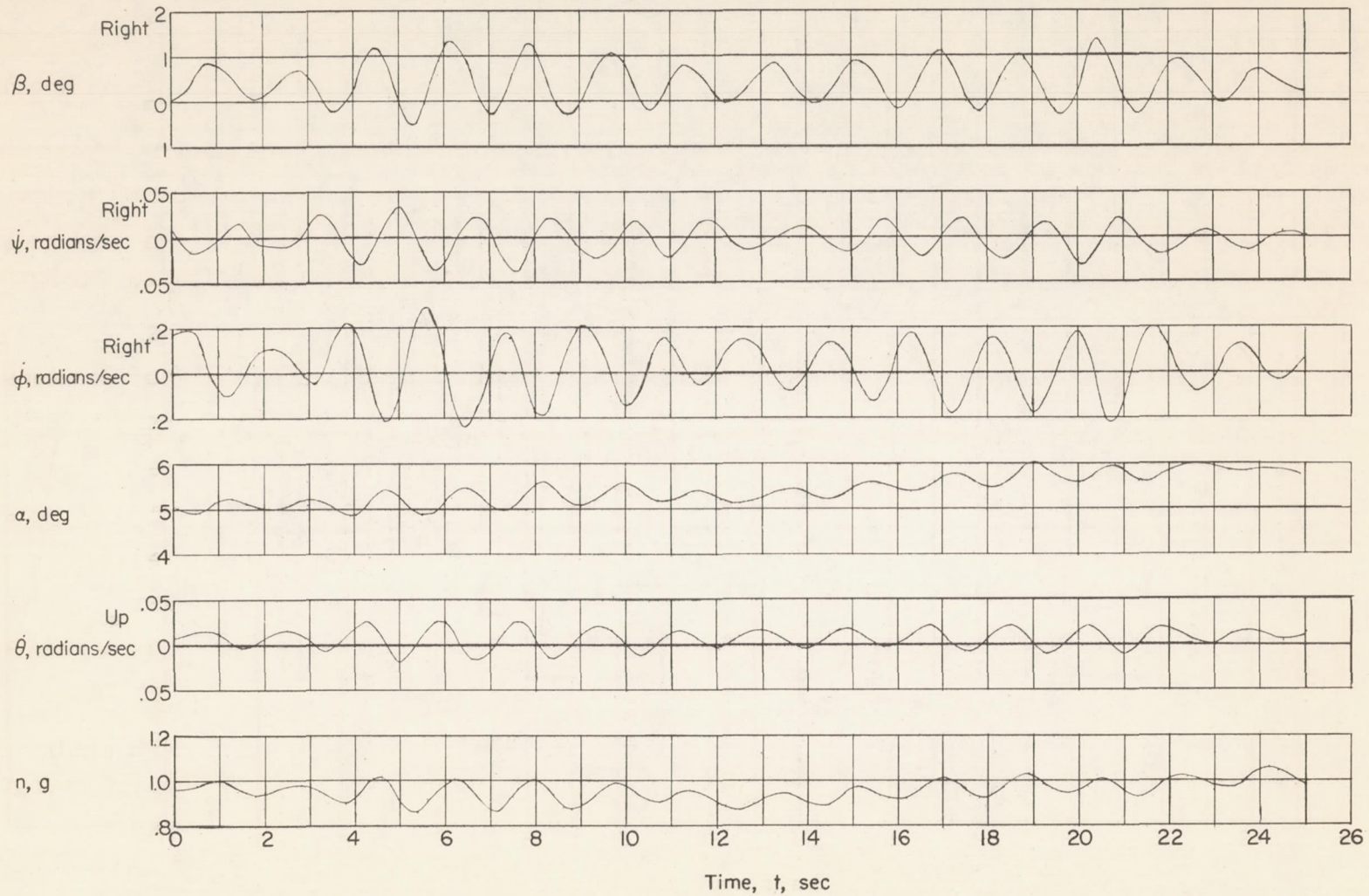


Figure 7.- Small amplitude undamped oscillation with all controls held fixed to less than 0.05° motion. $M = 0.88$; $h_p = 40,000$ feet.

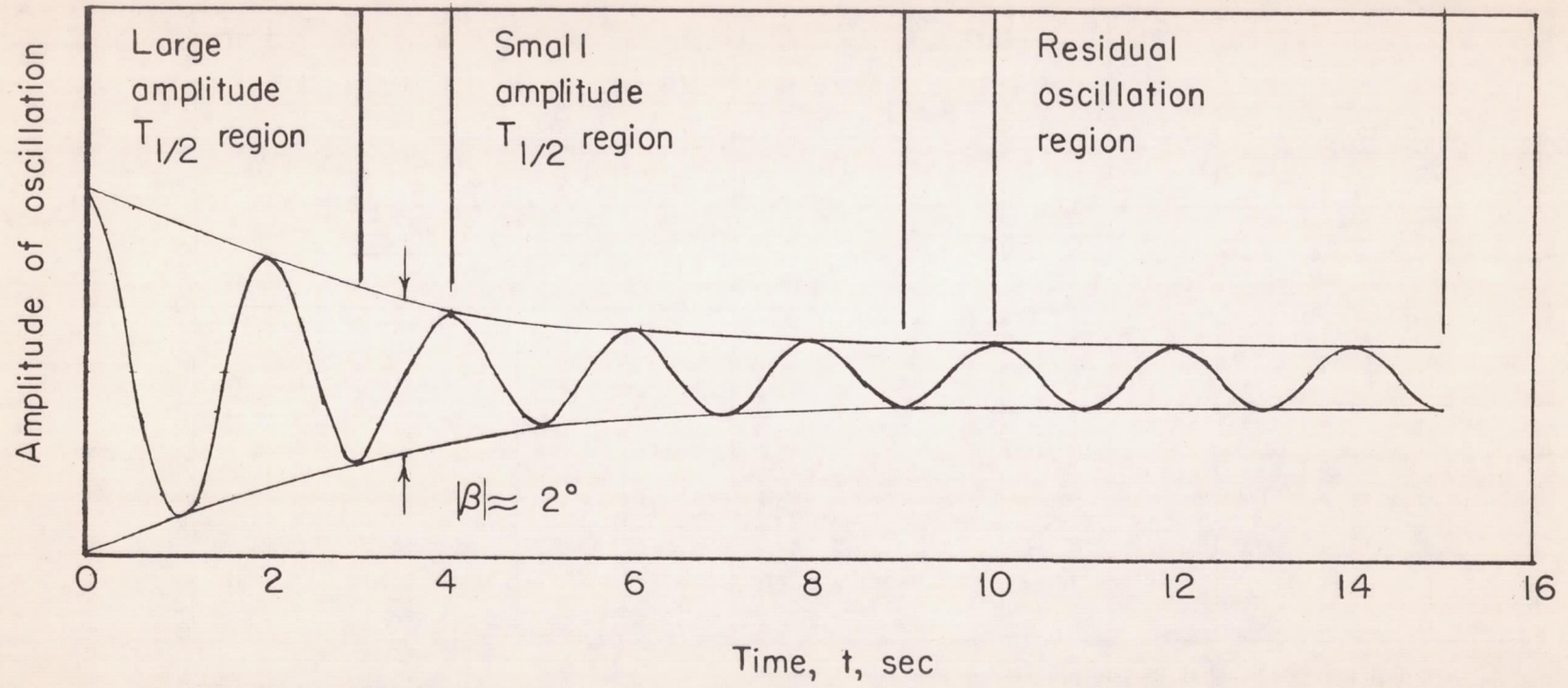
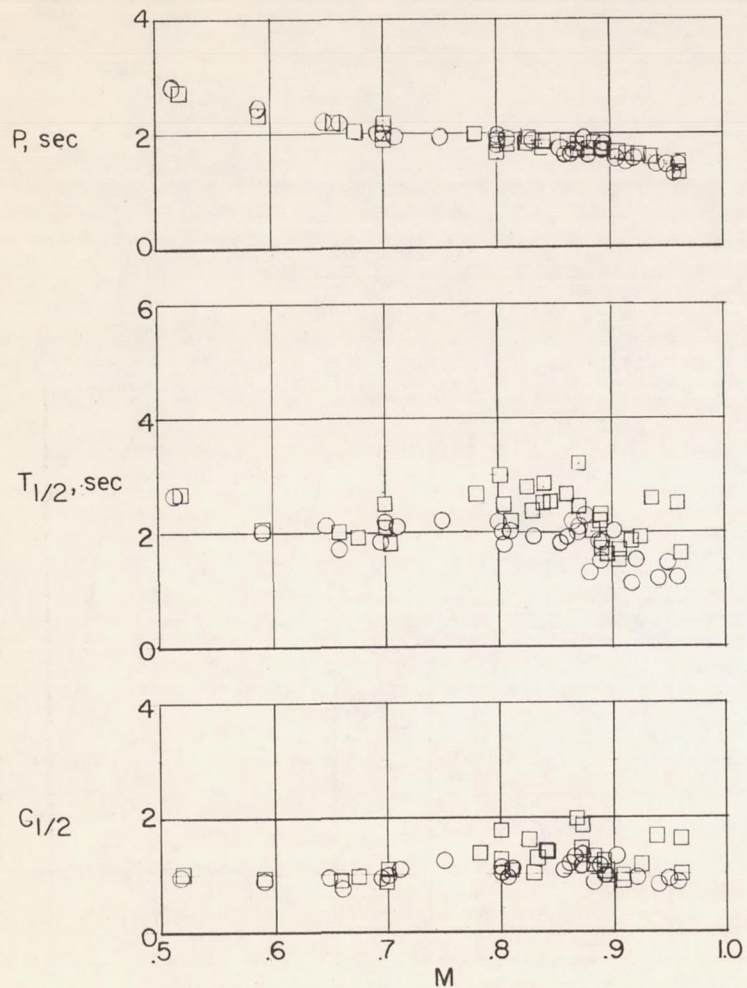
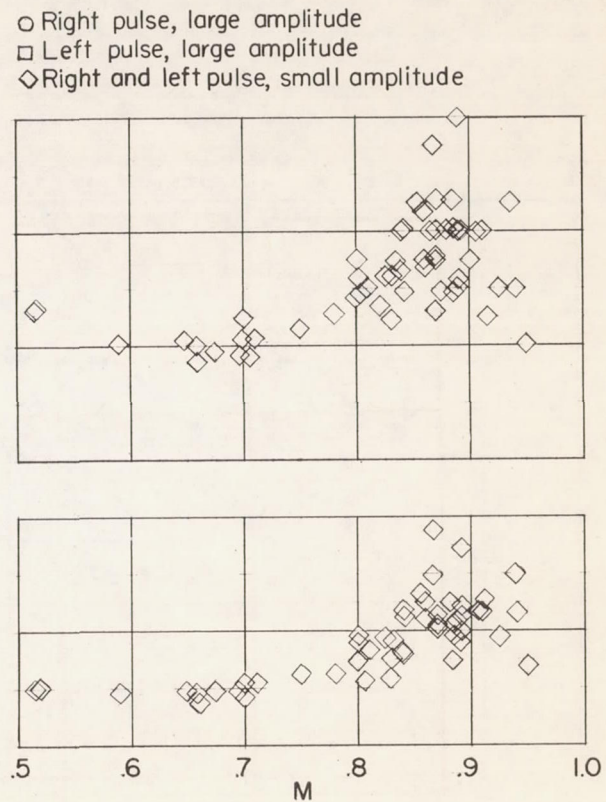


Figure 8.- Transient oscillation indicating various damping regions.



(a) Large amplitude.



(b) Small amplitude.

Figure 9.- Period and damping for the lateral response of the X-5 airplane to a rudder pulse input at 40,000 feet.

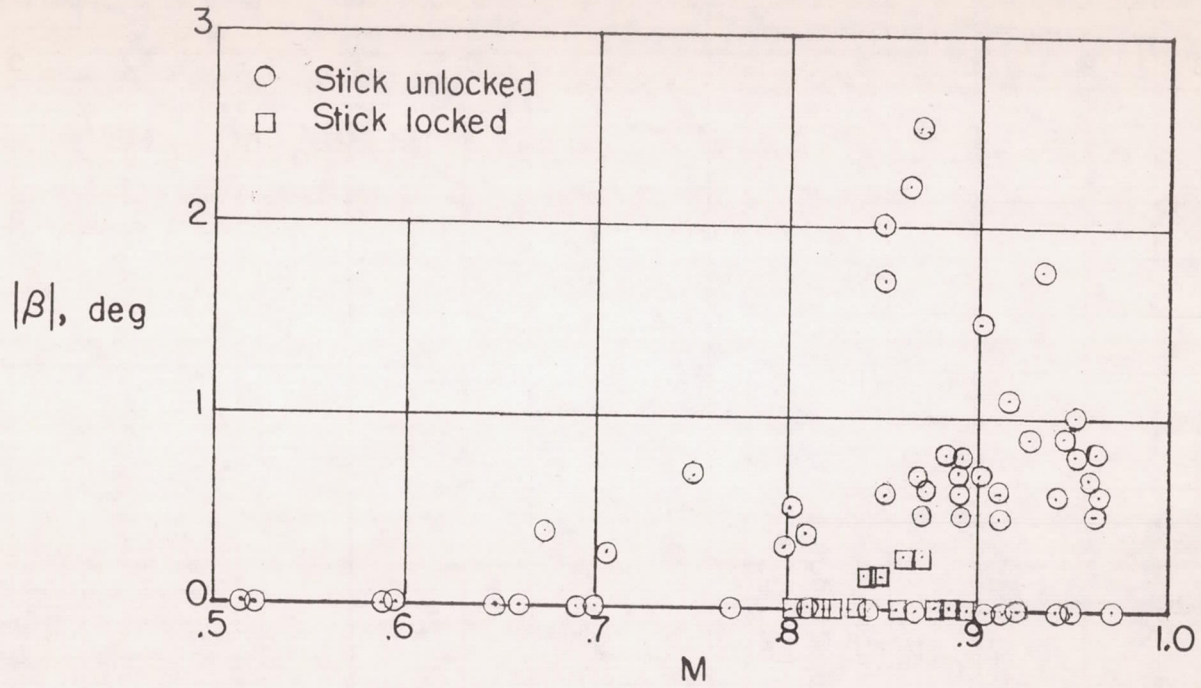


Figure 10.- Variation with Mach number of the amplitude of the residual lateral oscillation at 40,000 feet.

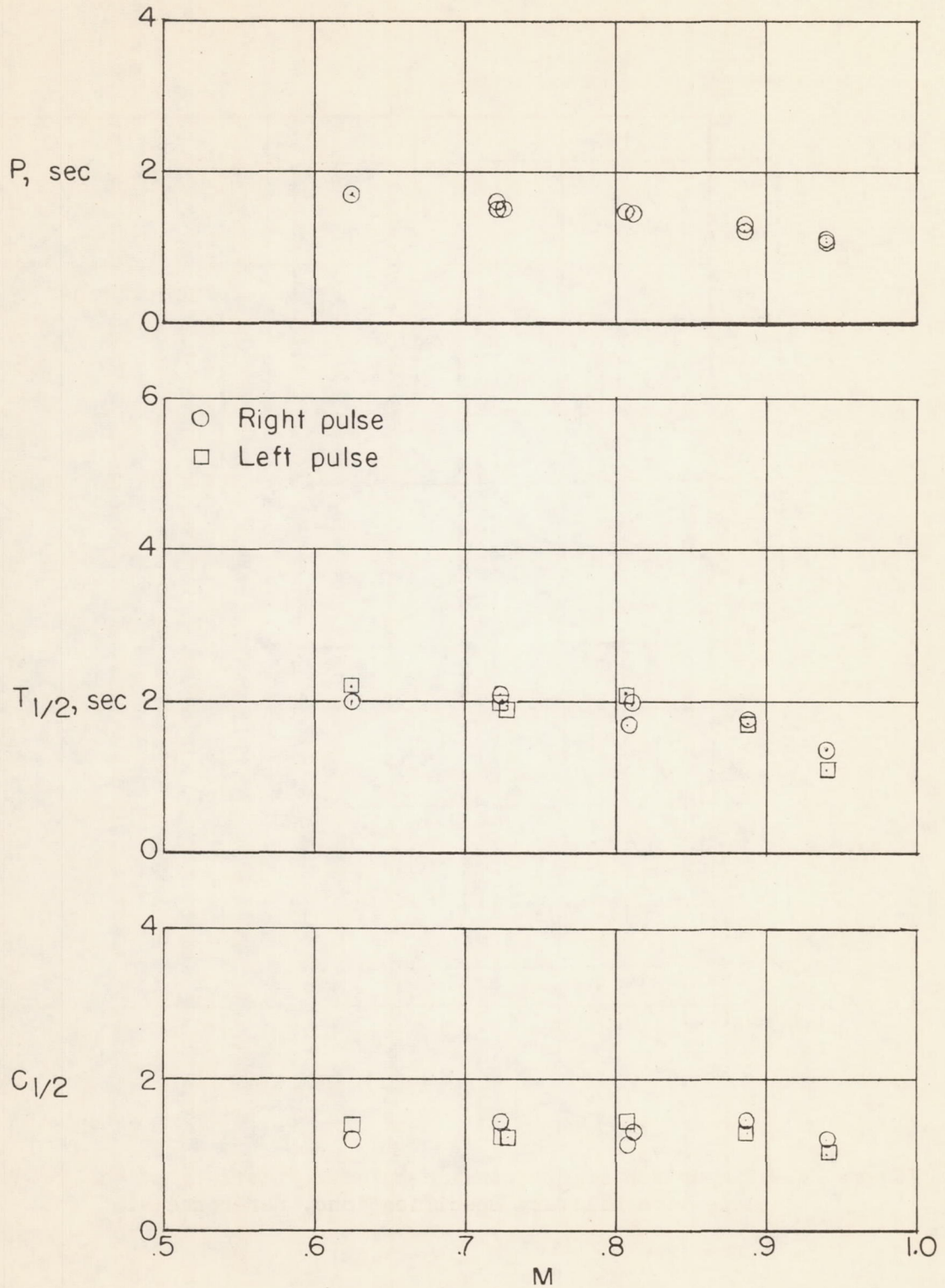


Figure 11.- Period and damping for the lateral response of the X-5 airplane to a rudder pulse input at 25,000 feet.

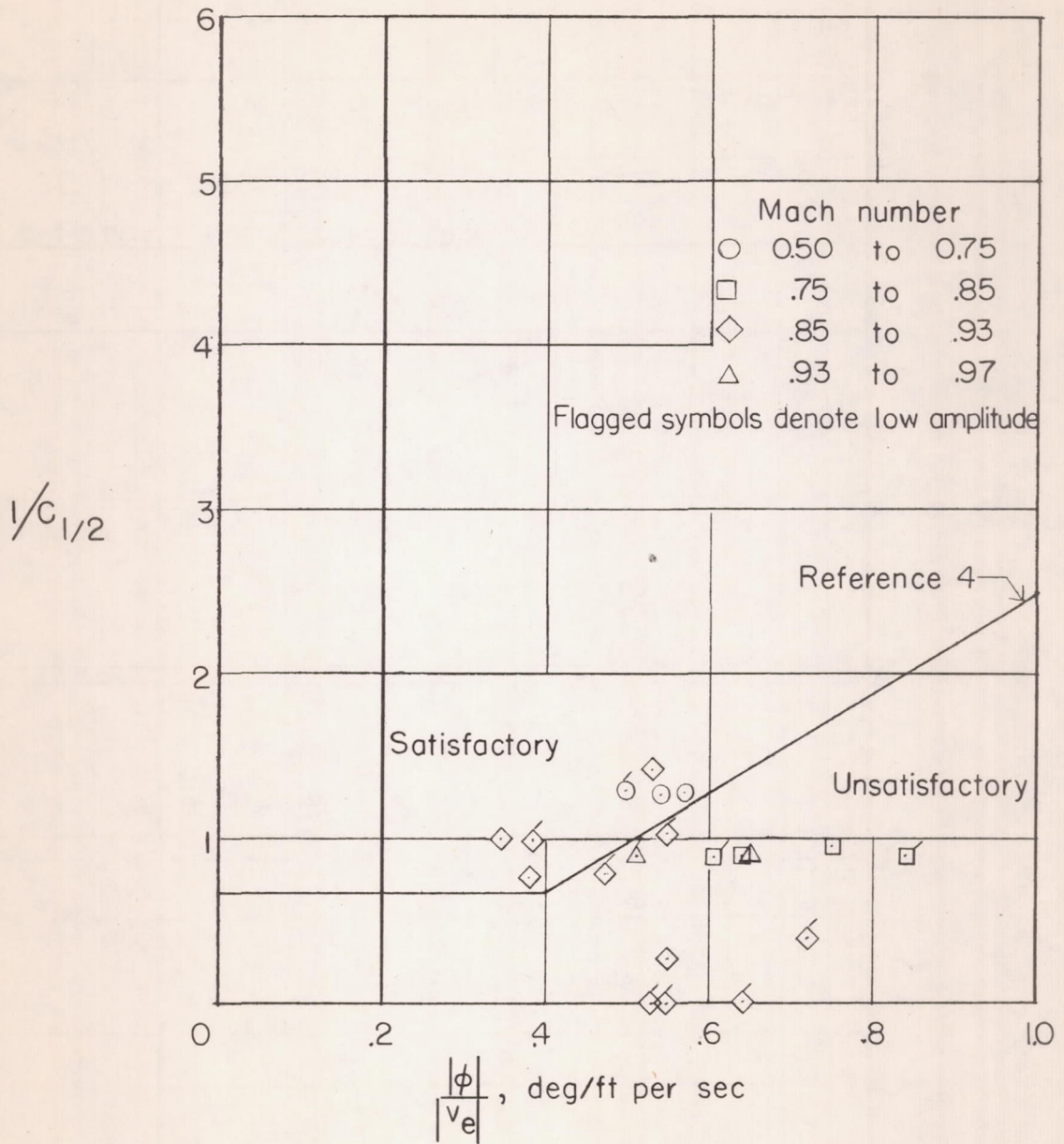


Figure 12.- Comparison of the dynamic lateral stability of the X-5 airplane with Military Specifications, reference 4.

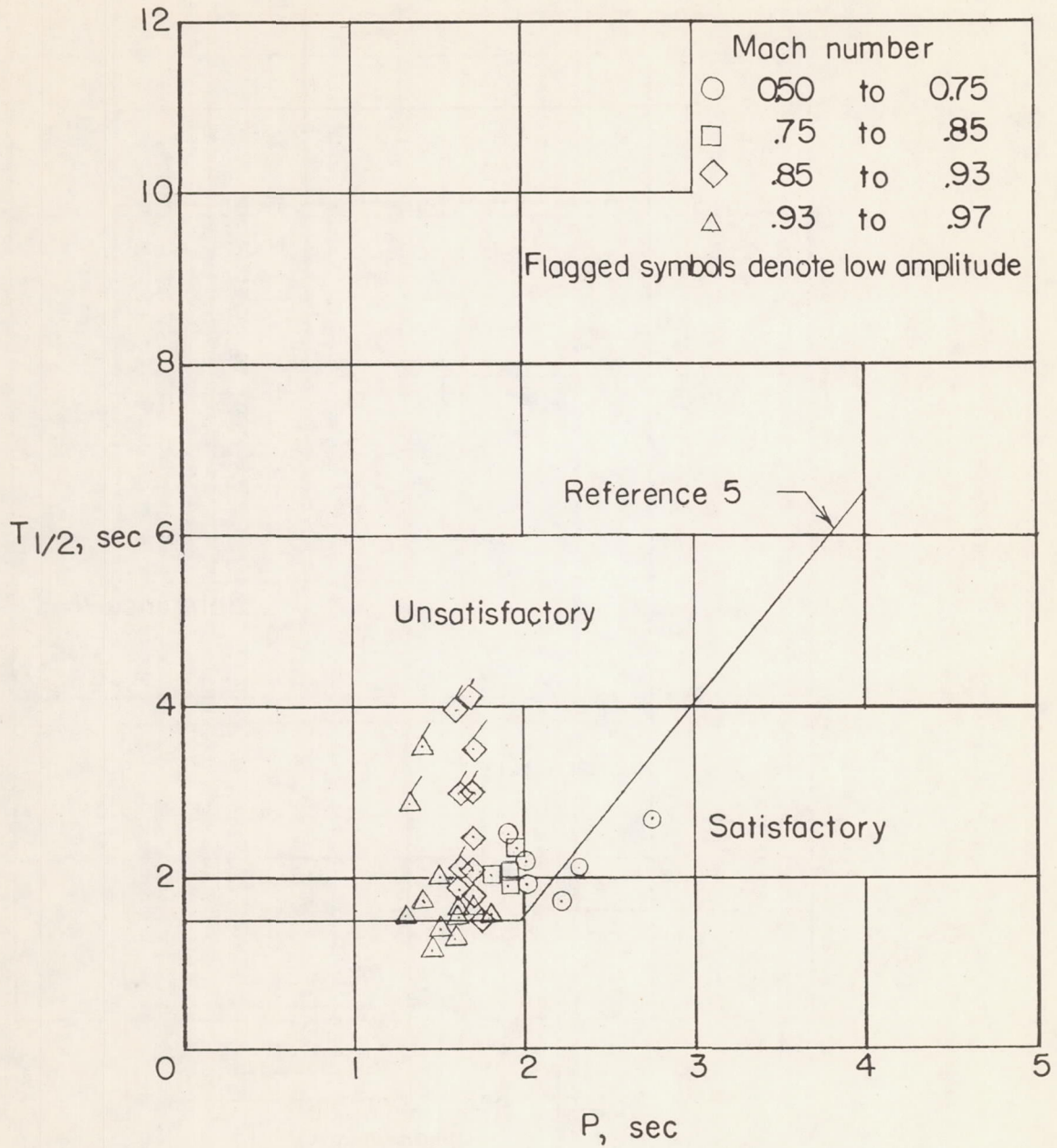
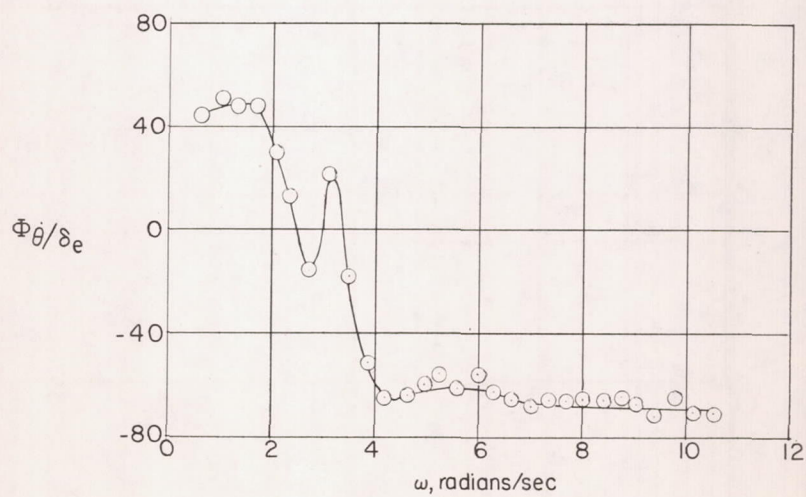
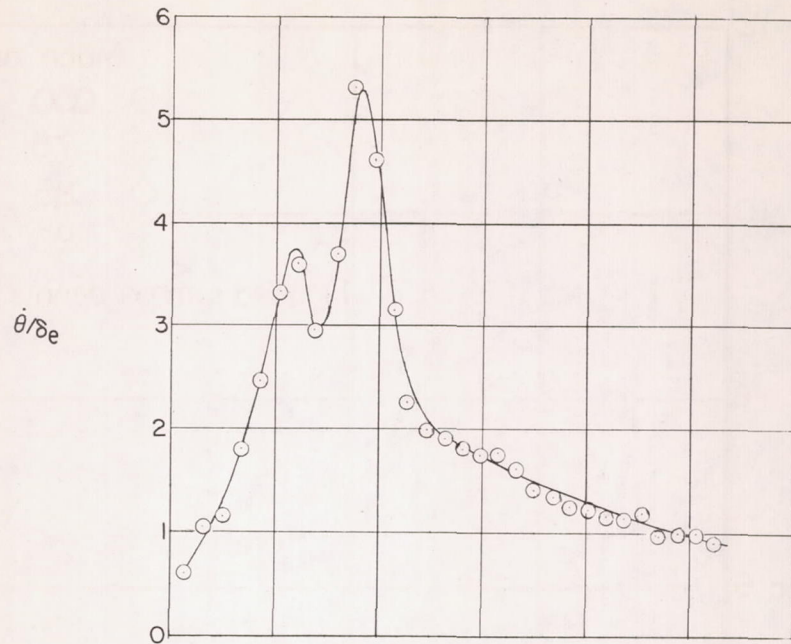
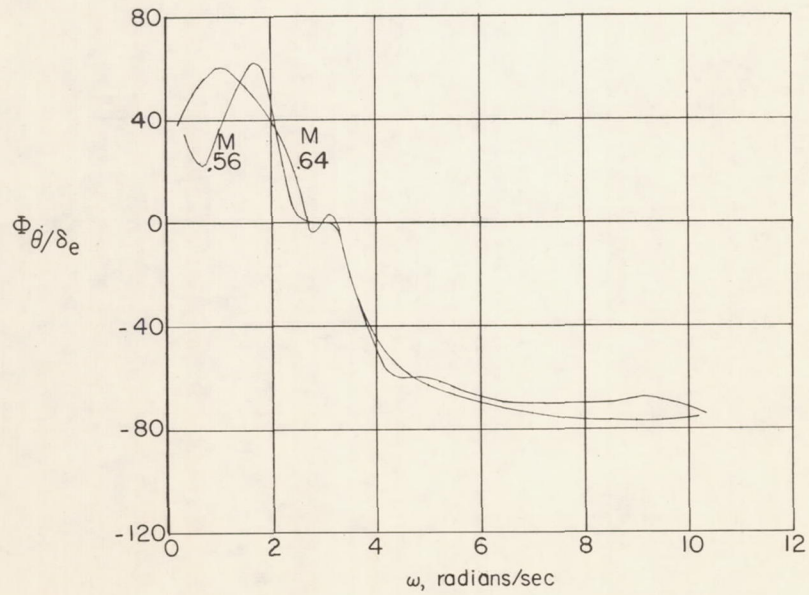
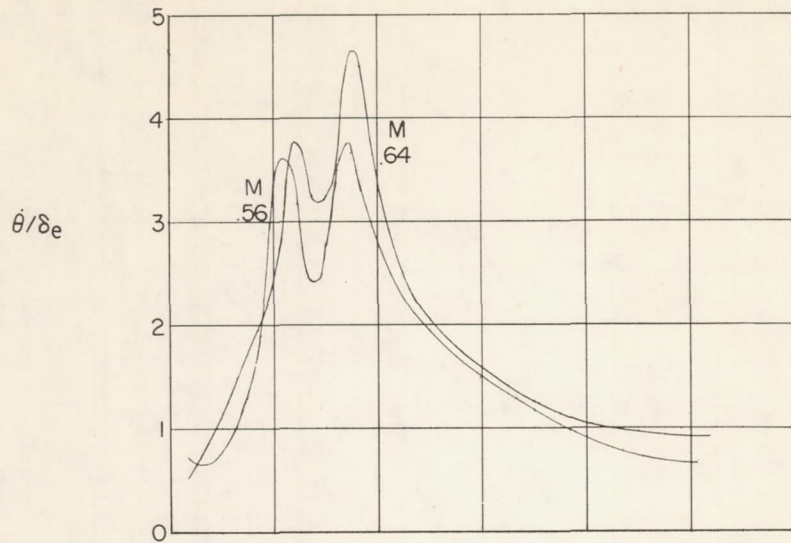


Figure 13.- Comparison of the lateral dynamic stability of the X-5 airplane with superseded Air Force criteria, reference 5.



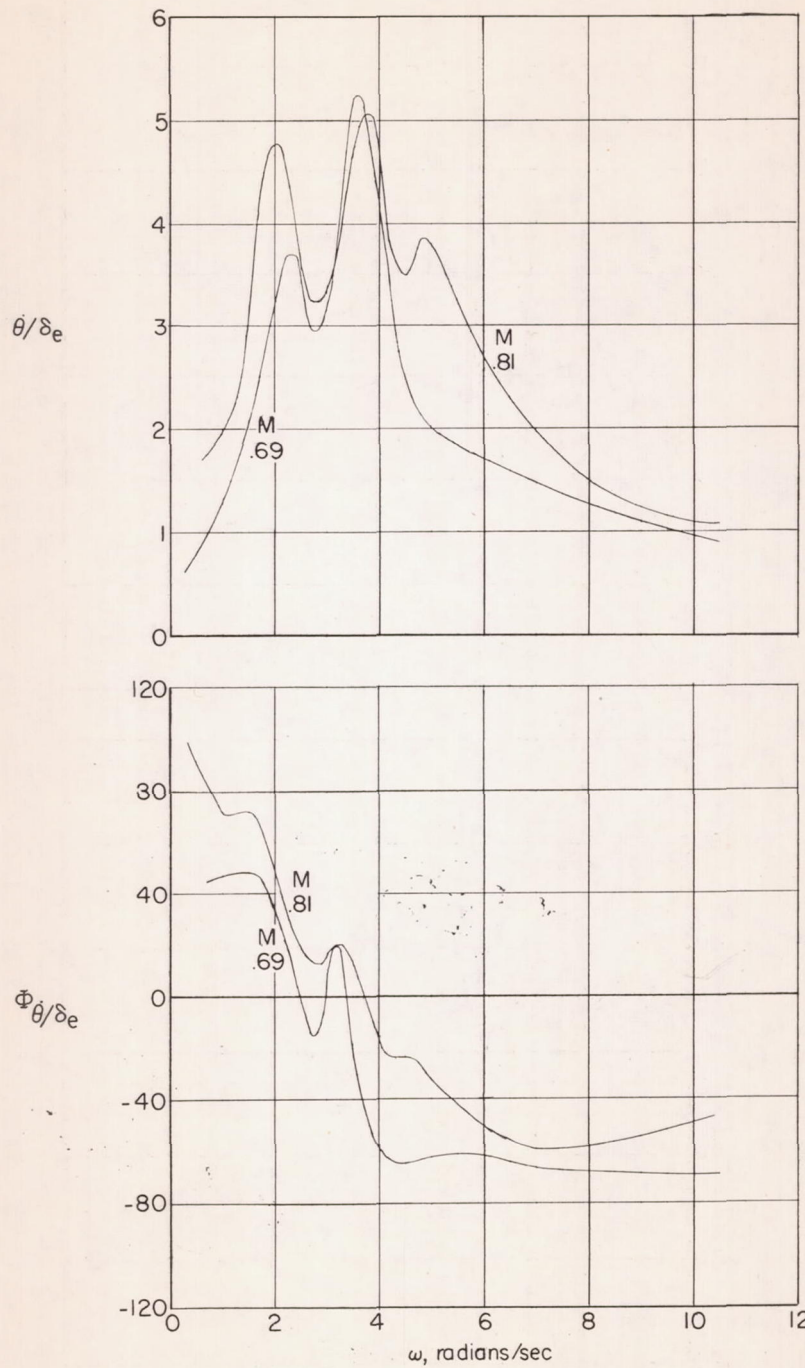
(a) Sample calculation showing calculated frequency response points.
 $M = 0.69$; $h_p = 40,000$ feet.

Figure 14.- Longitudinal frequency response as calculated from longitudinal transient responses.



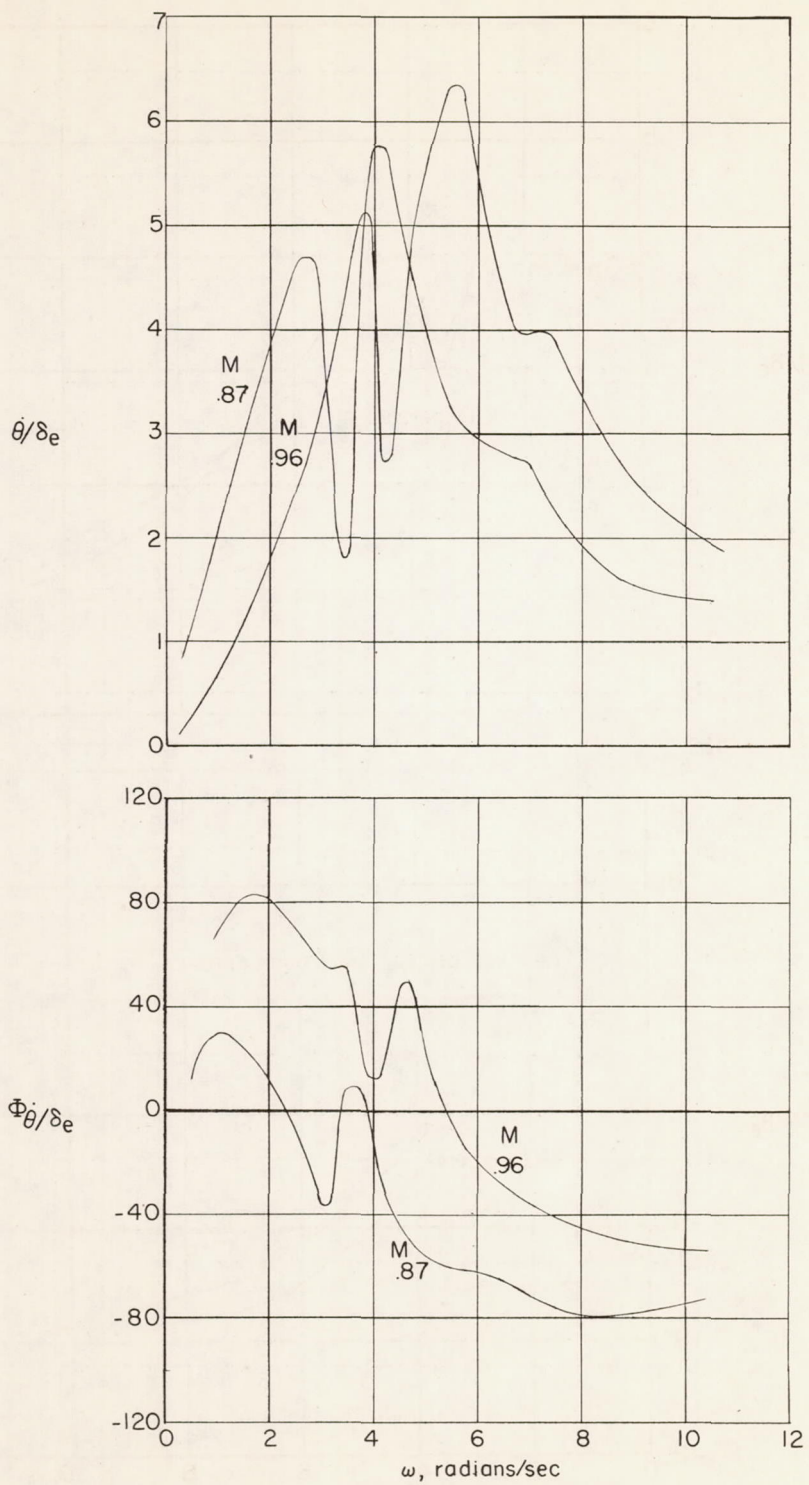
(b)

Figure 14.- Continued.



(c)

Figure 14.- Continued.



(d)

Figure 14.- Concluded.

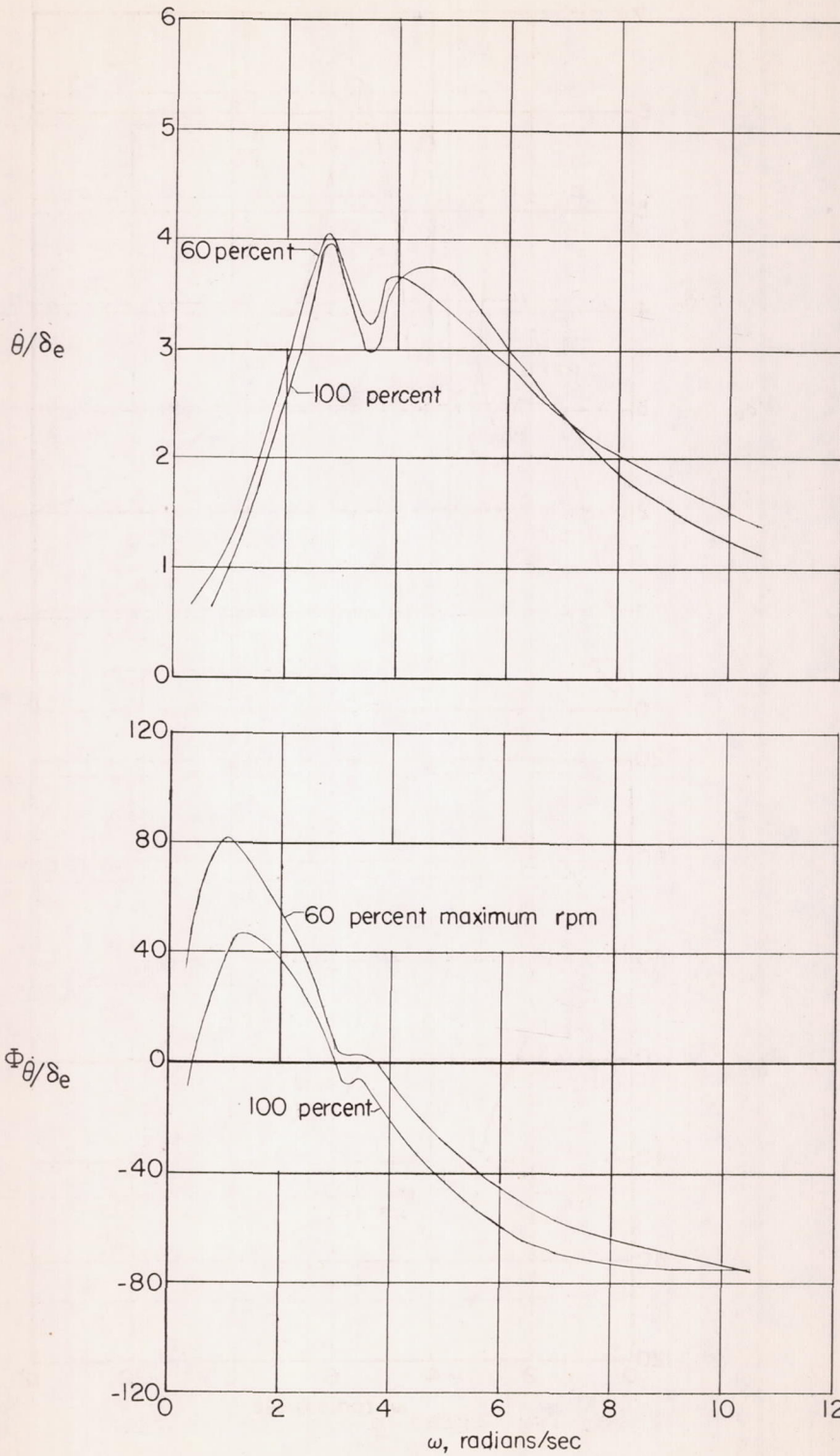
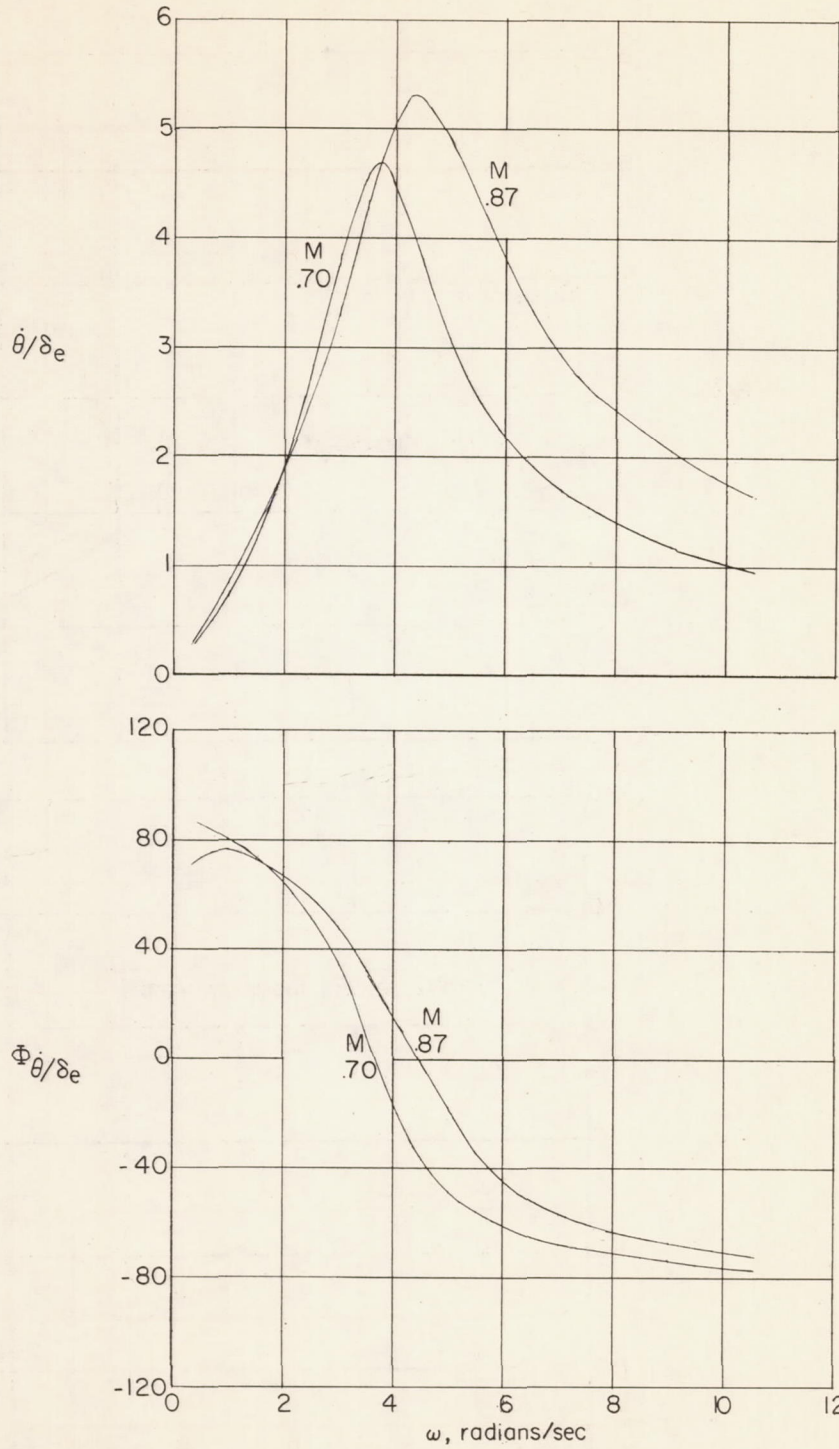
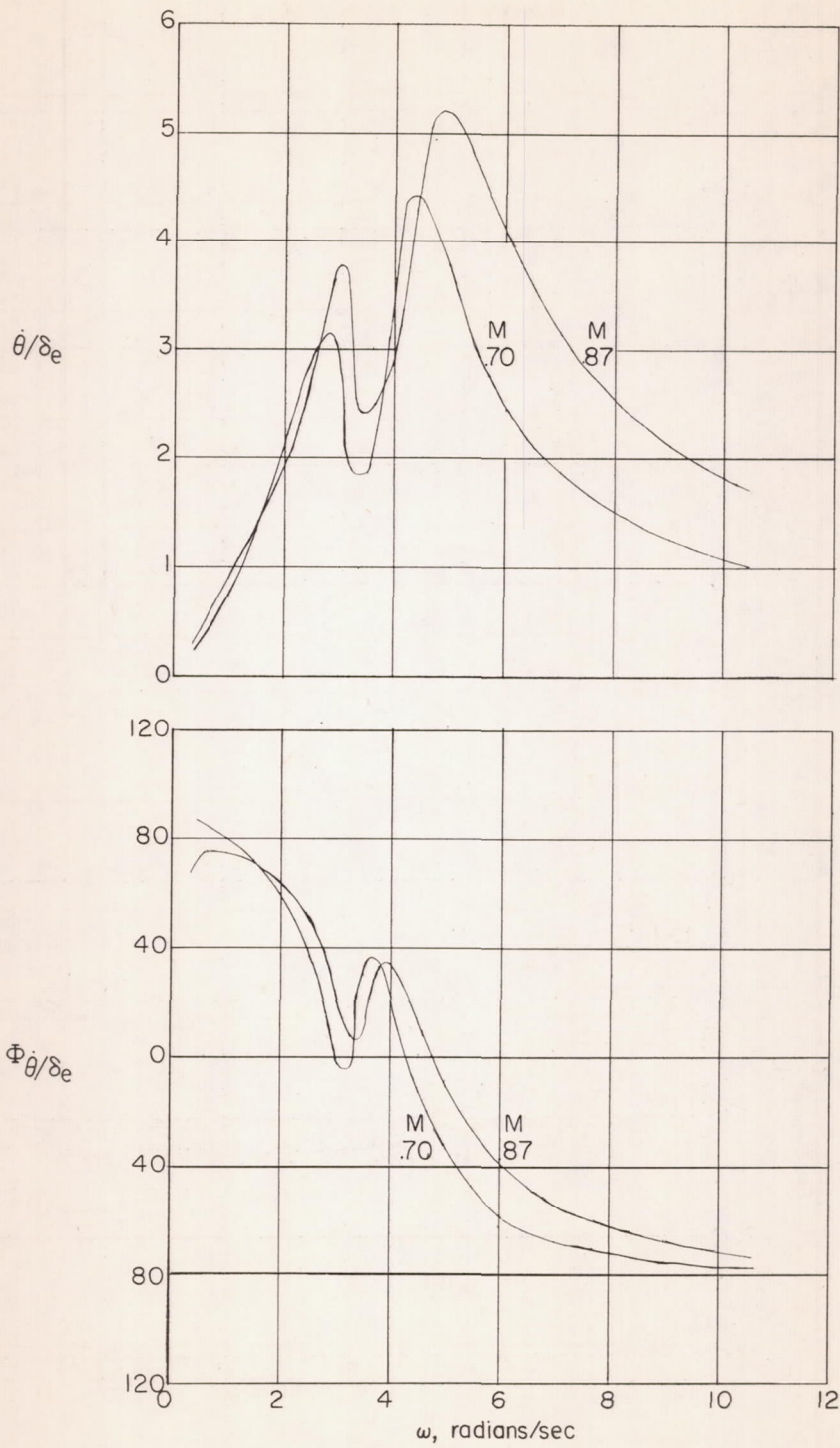


Figure 15.- Longitudinal frequency response with engine idling and at maximum rpm at 15,000 feet and Mach number of 0.6.



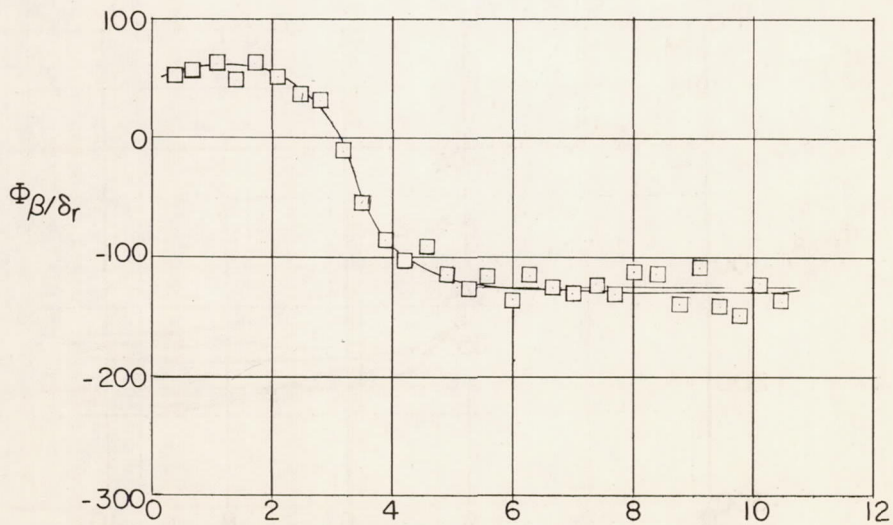
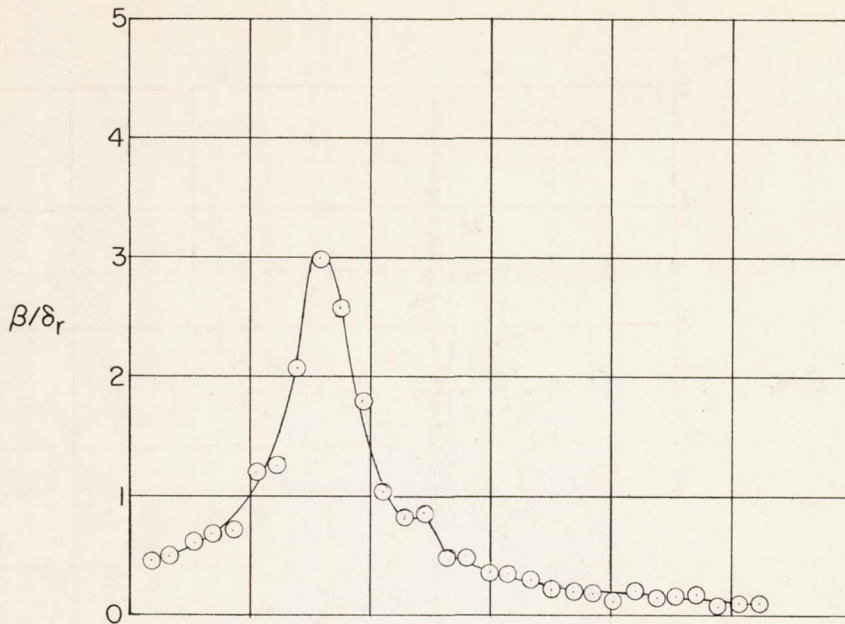
(a) Two degree-of-freedom system.

Figure 16.- Longitudinal frequency response calculated from theoretical transfer function. $h_p = 40,000$ feet.



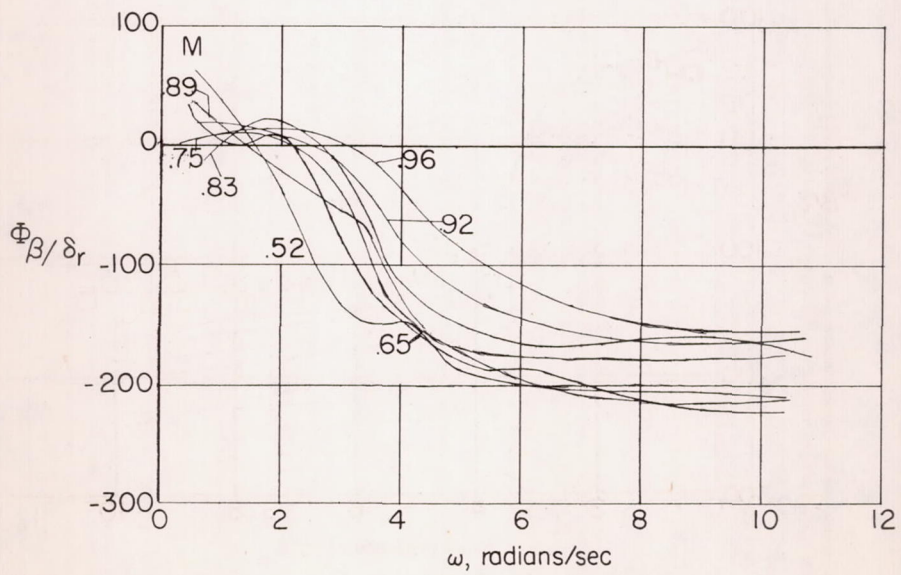
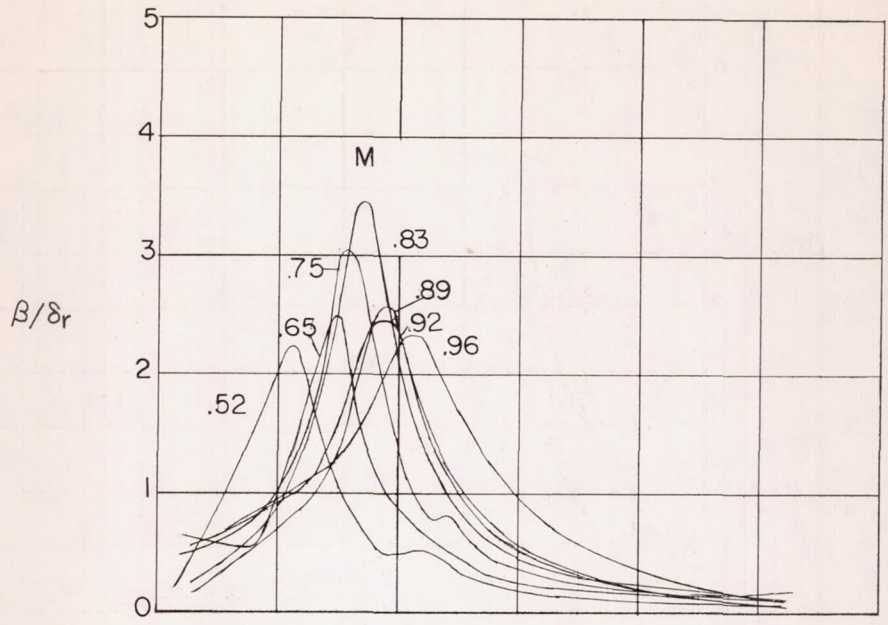
(b) Three-degree-of-freedom system.

Figure 16.- Concluded.



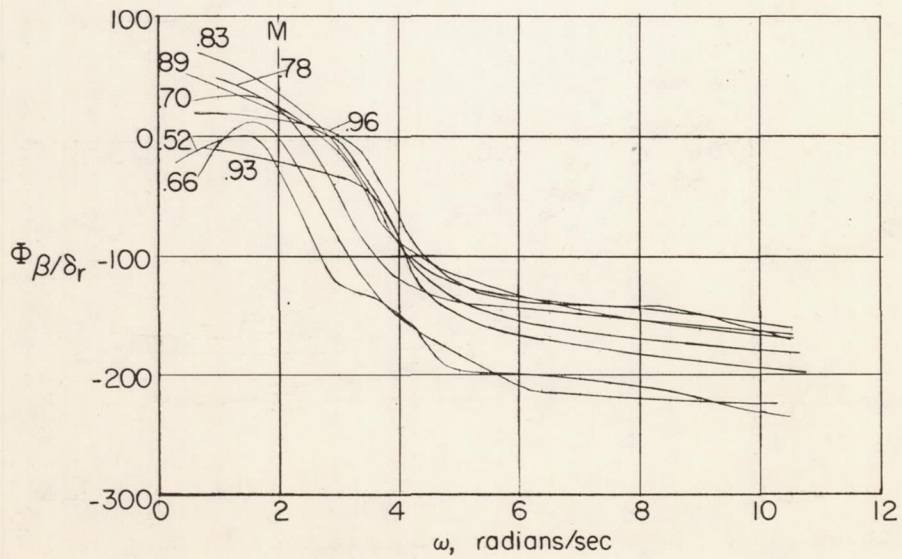
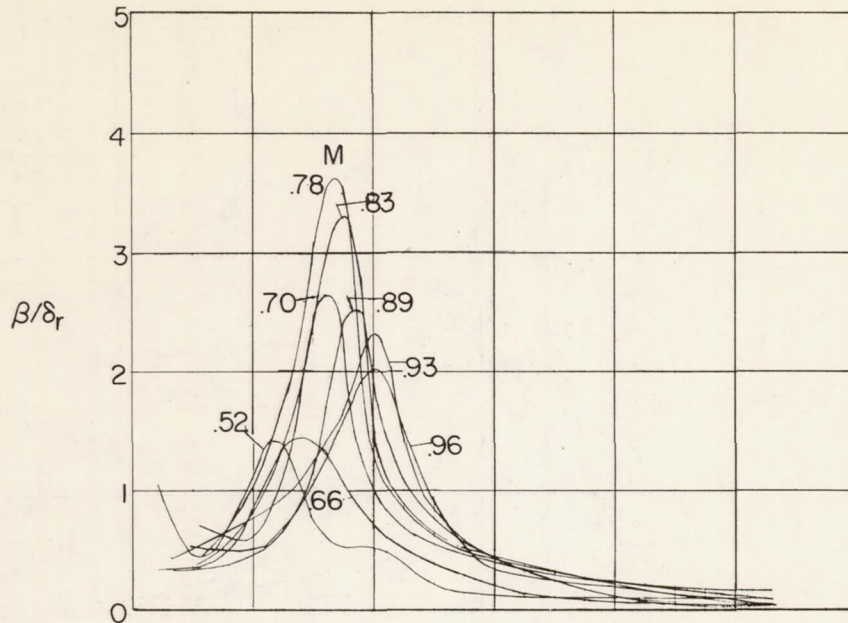
(a) Sample calculation showing calculated frequency response points at $M = 0.75$; $h_p = 40,000$ feet.

Figure 17.- Lateral frequency response β/δ_r as calculated from lateral transient responses.



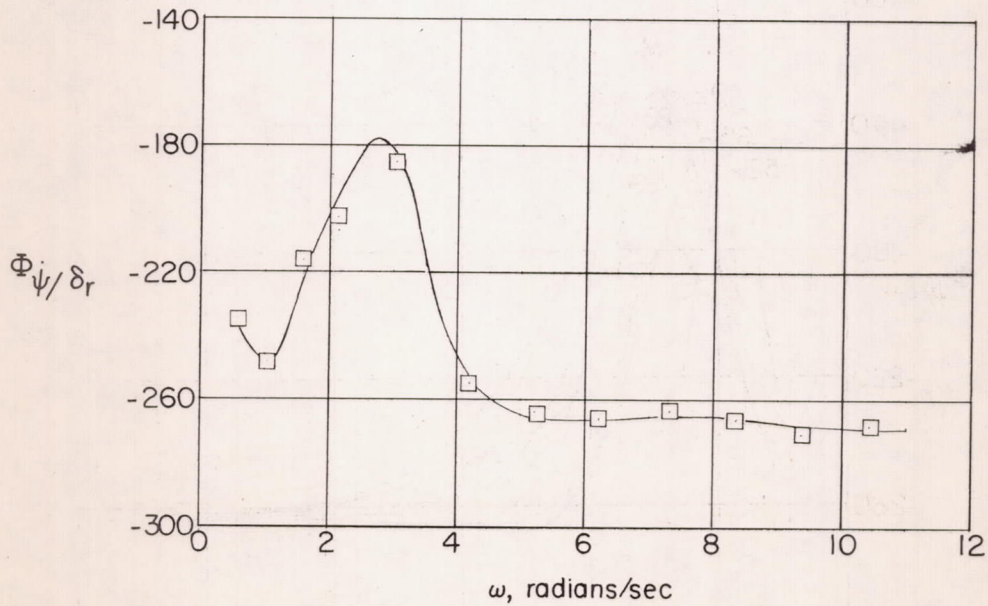
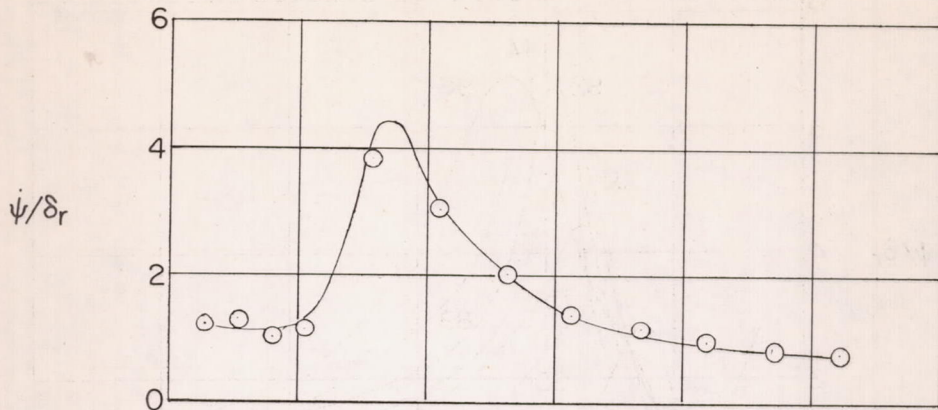
(b) Frequency response for right rudder pulses.

Figure 17.- Continued.



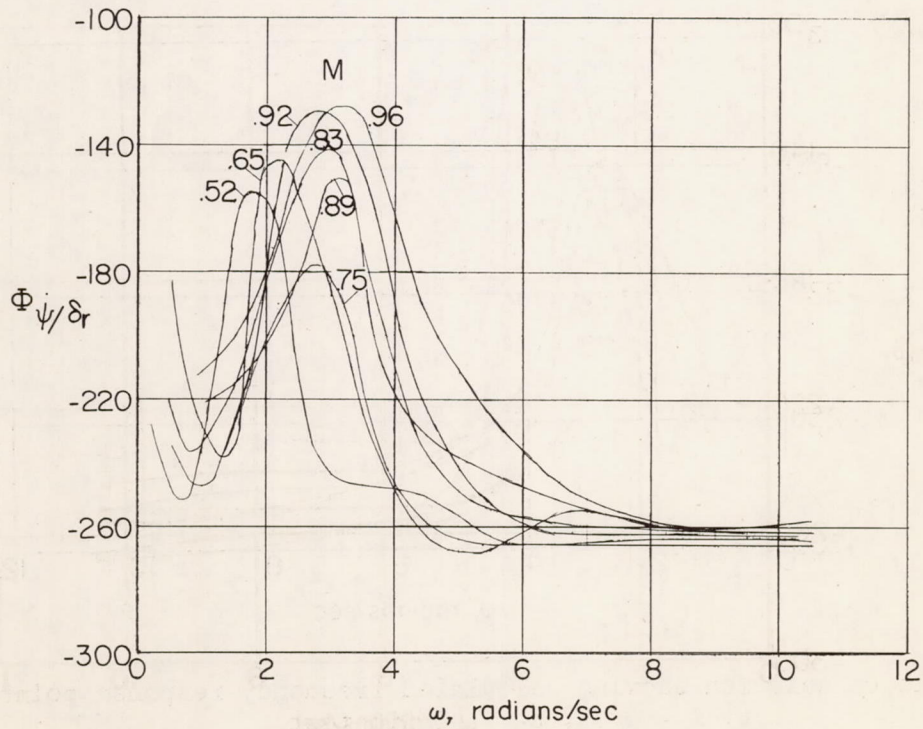
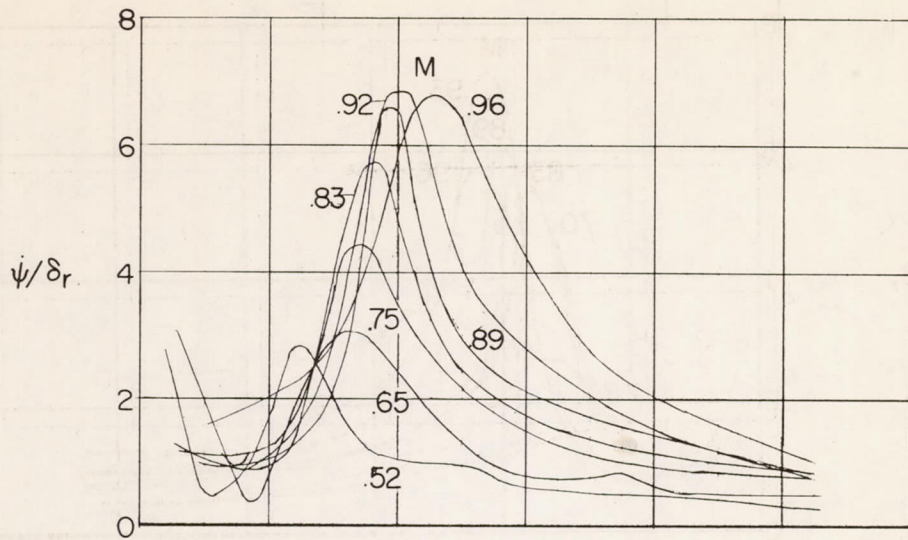
(c) Frequency response for left rudder pulses.

Figure 17.- Concluded.



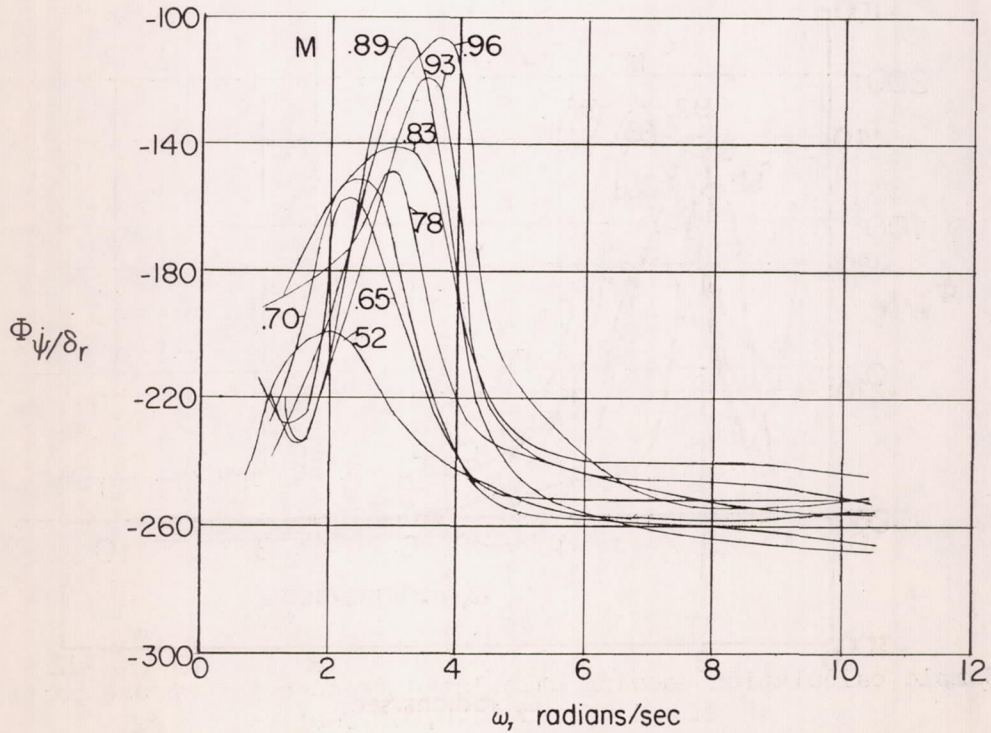
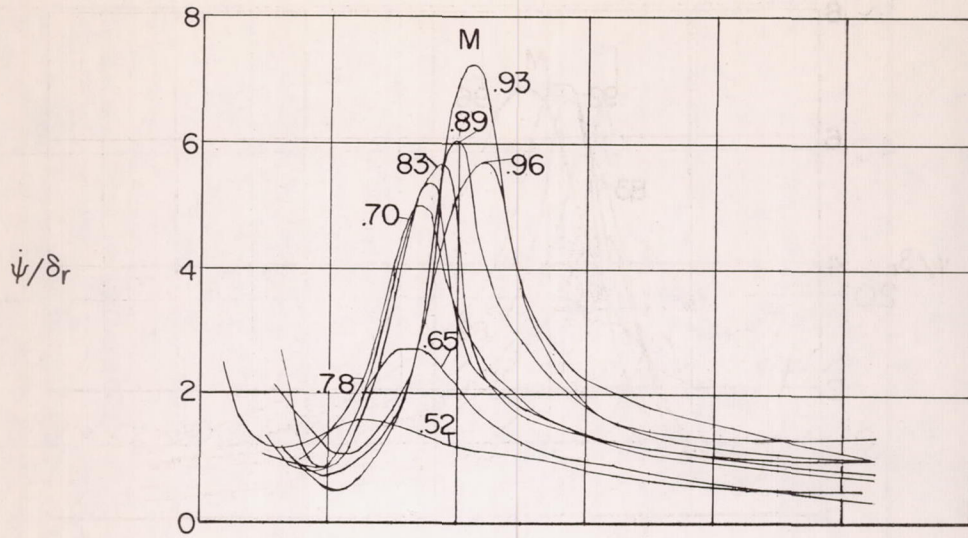
(a) Sample calculation showing calculated frequency response points at $M = 0.75$; $h_p = 40,000$ feet.

Figure 18.- Lateral frequency response $\dot{\psi}/\delta_r$ as calculated from lateral transient responses.



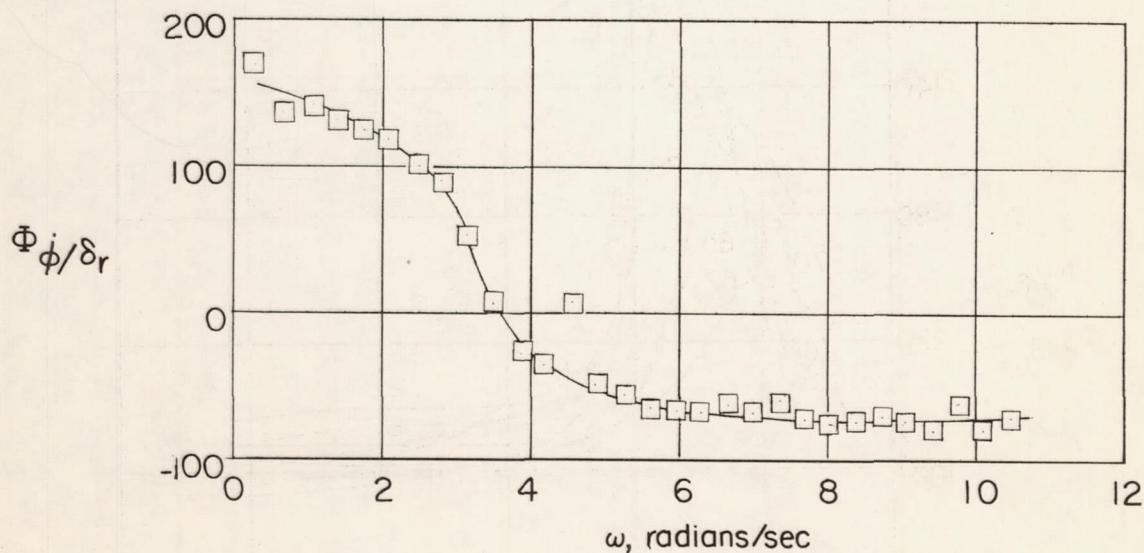
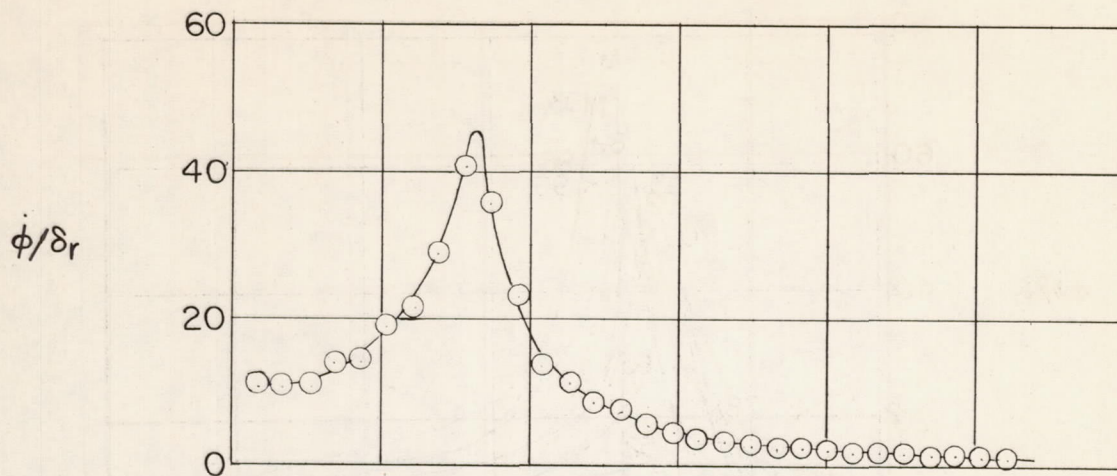
(b) Frequency response of right rudder pulses.

Figure 18.- Continued.



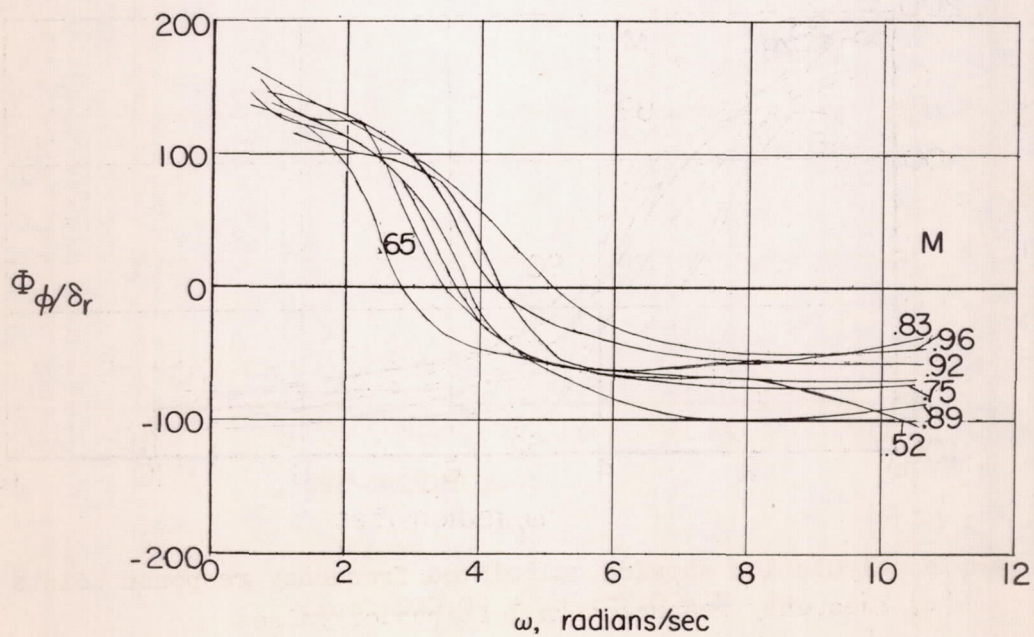
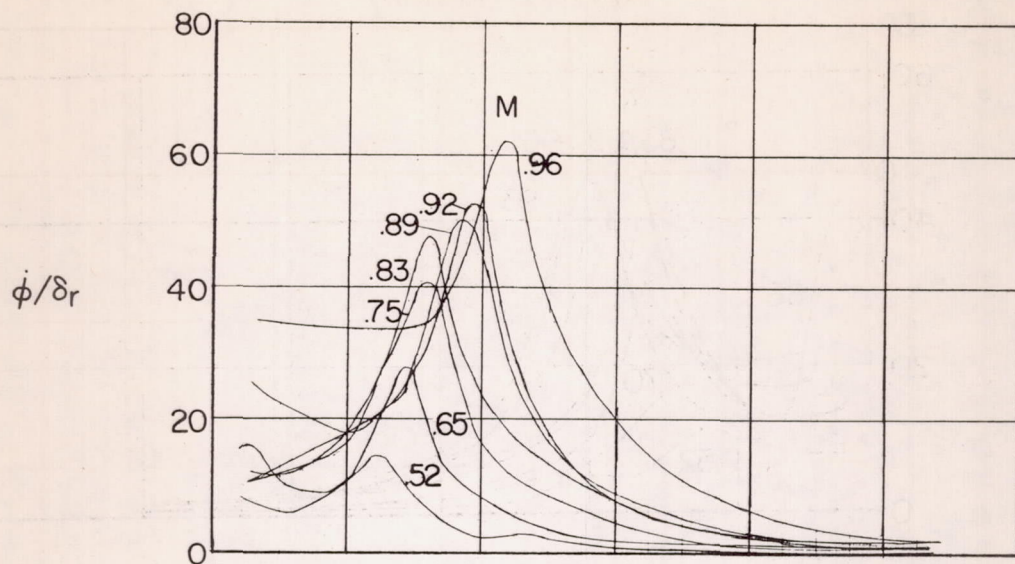
(c) Frequency response of left rudder pulses.

Figure 18.- Concluded.



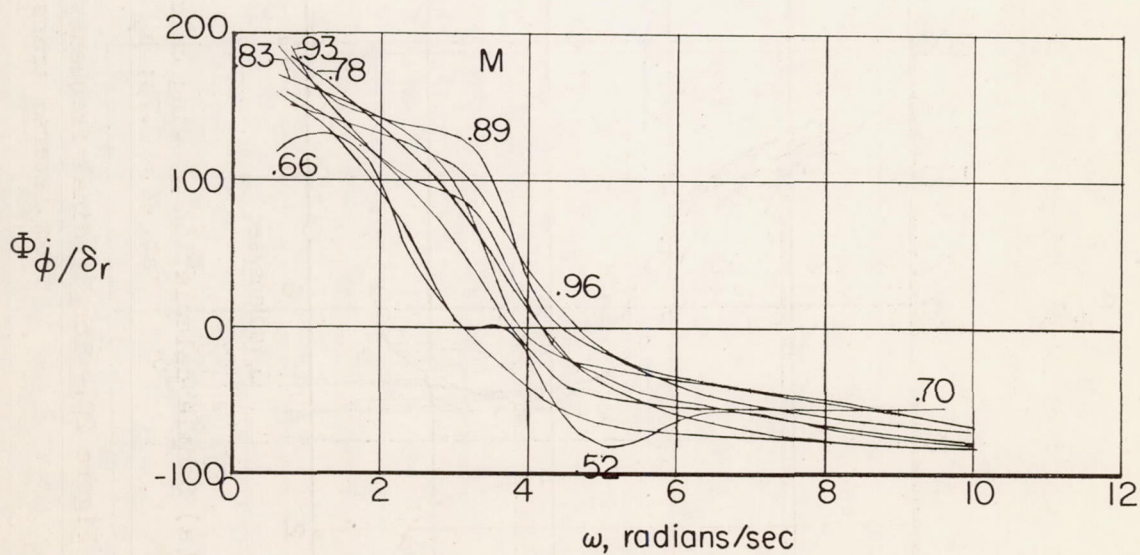
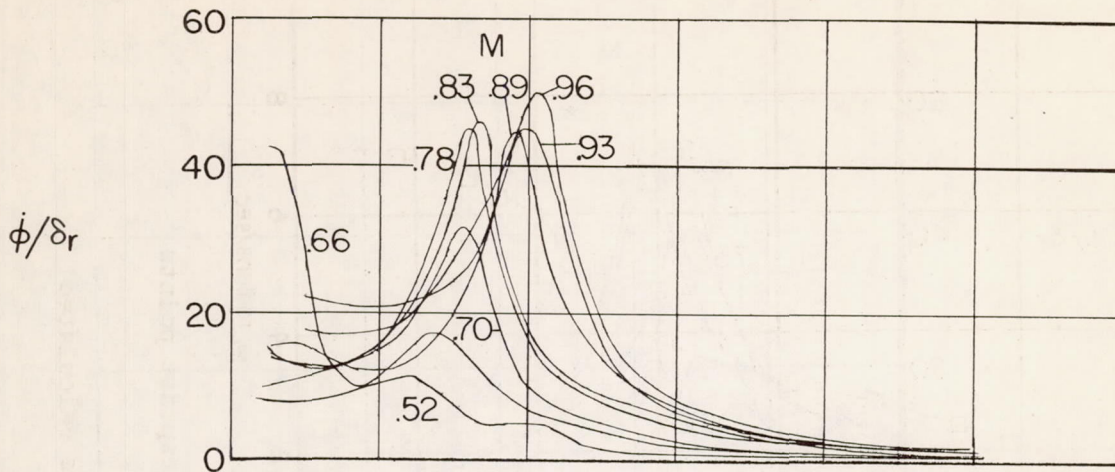
(a) Sample calculation showing calculated frequency response points at $M = 0.75$; $h_p = 40,000$ feet.

Figure 19.- Lateral frequency response $\dot{\phi}/\delta_r$ as calculated from lateral transient responses.



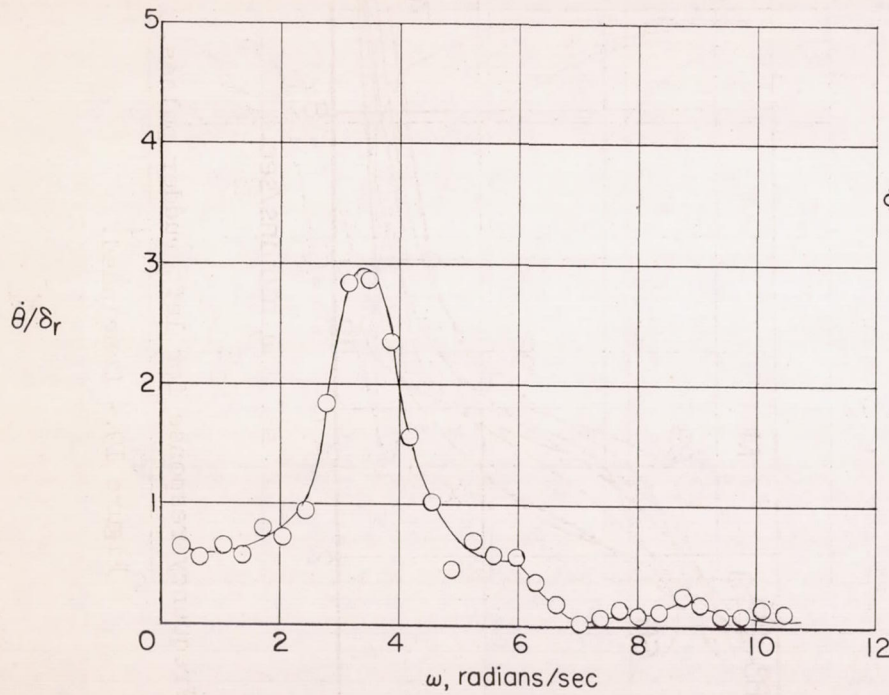
(b) Frequency response for right rudder pulses.

Figure 19.- Continued.



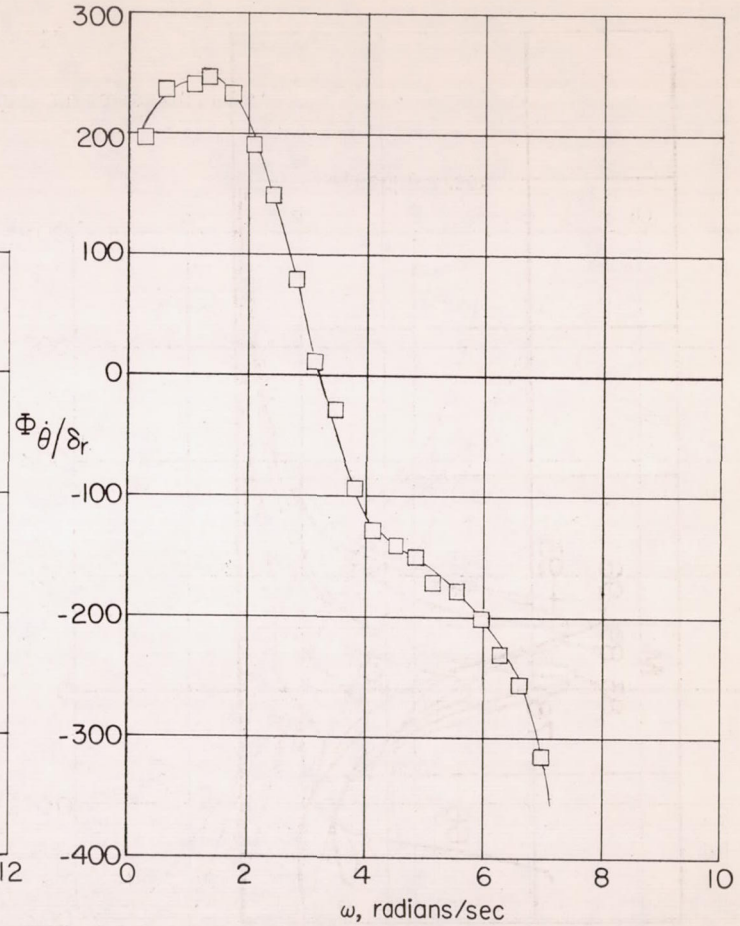
(c) Frequency response for left rudder pulses.

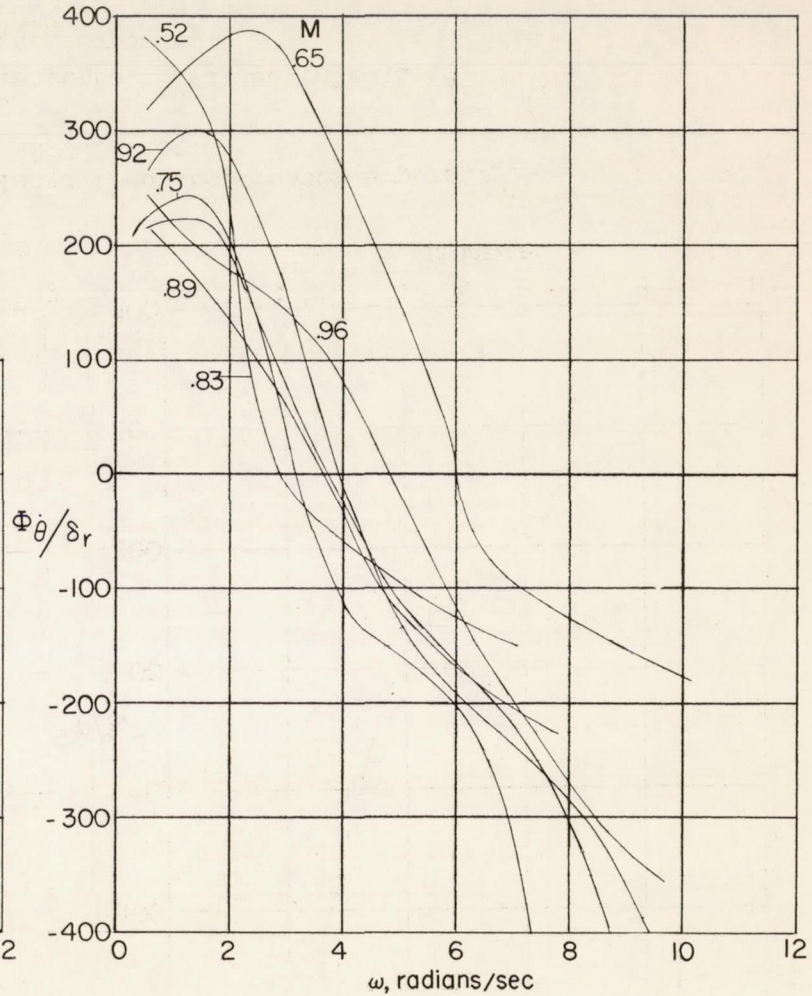
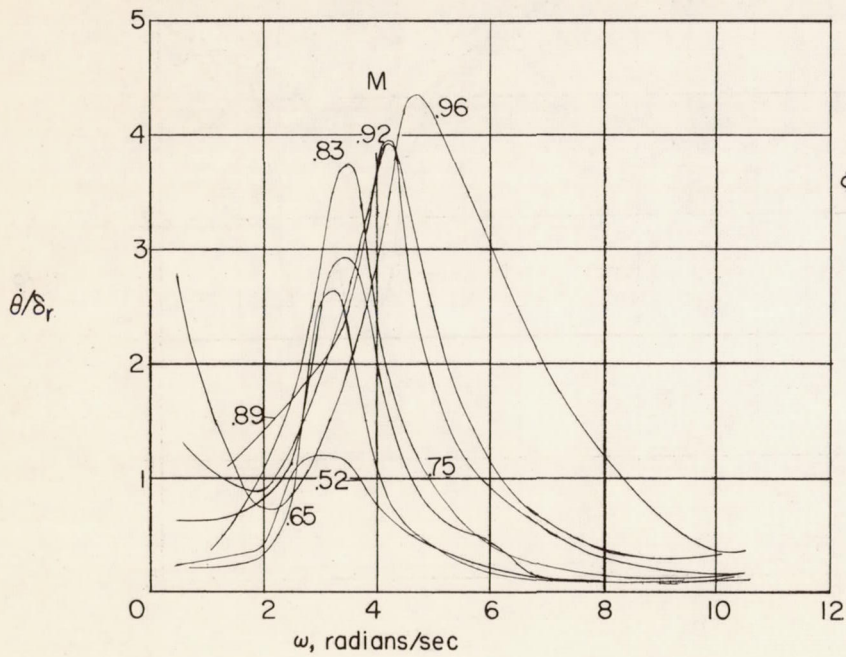
Figure 19.- Concluded.



(a) Sample calculation showing calculated frequency response points at $M = 0.75$; $h_p = 40,000$ feet.

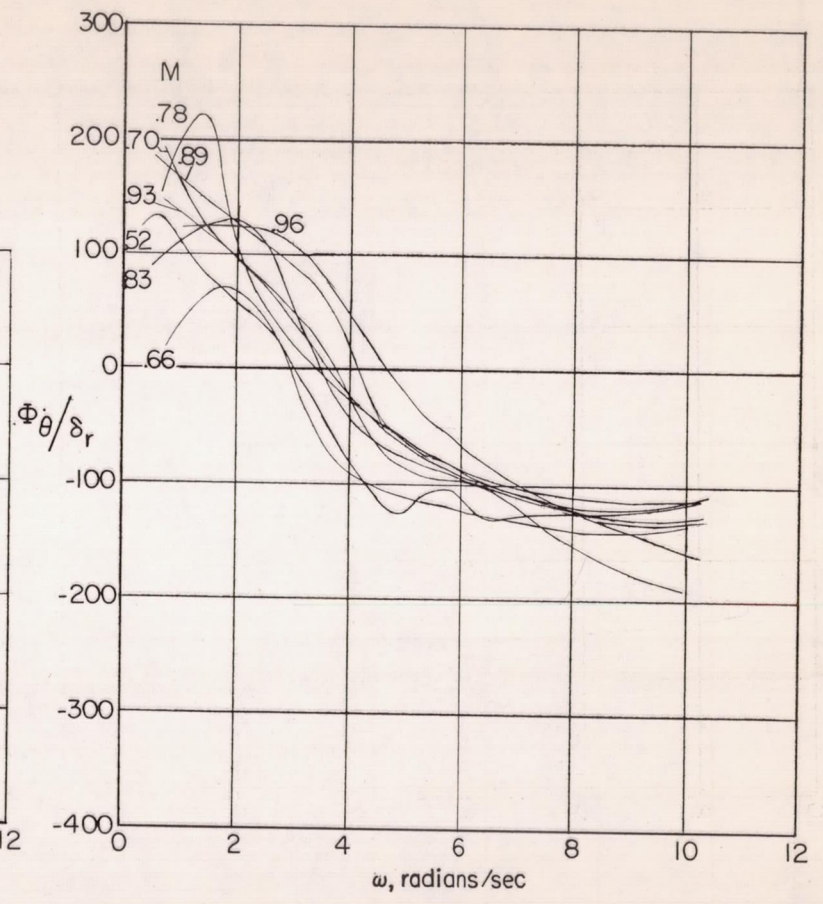
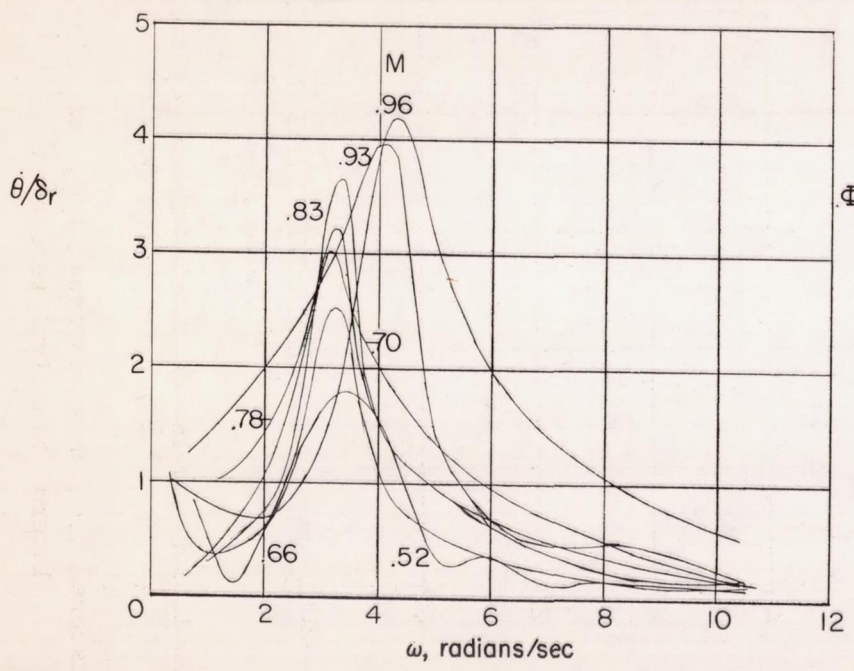
Figure 20.- Longitudinal frequency response $\dot{\theta}/\delta_r$ as calculated from lateral transient responses.





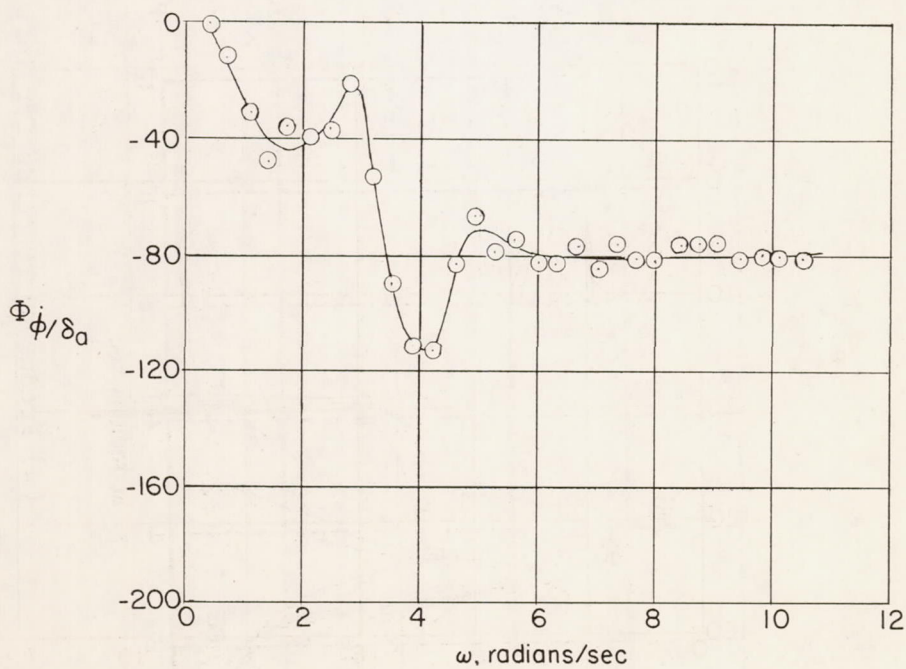
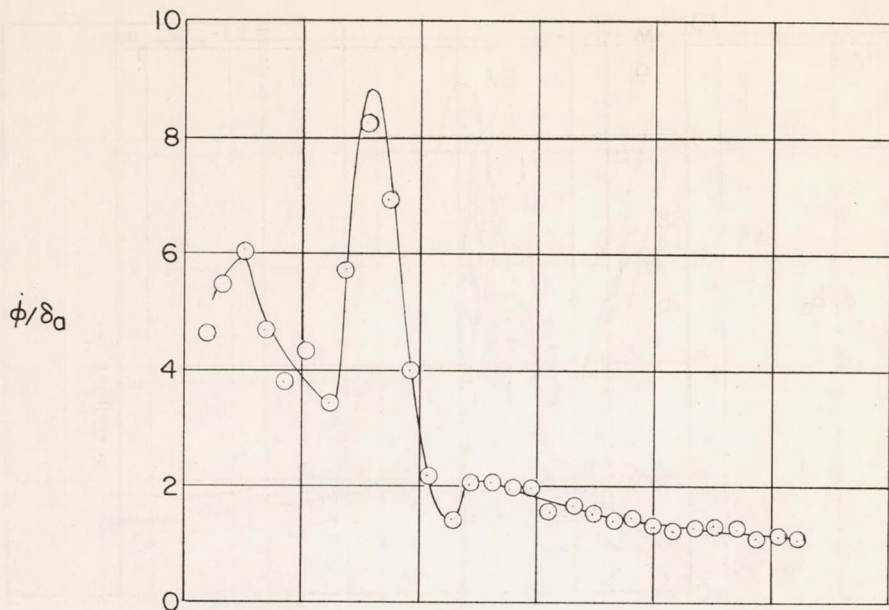
(b) Frequency response for right rudder pulses.

Figure 20.- Continued.



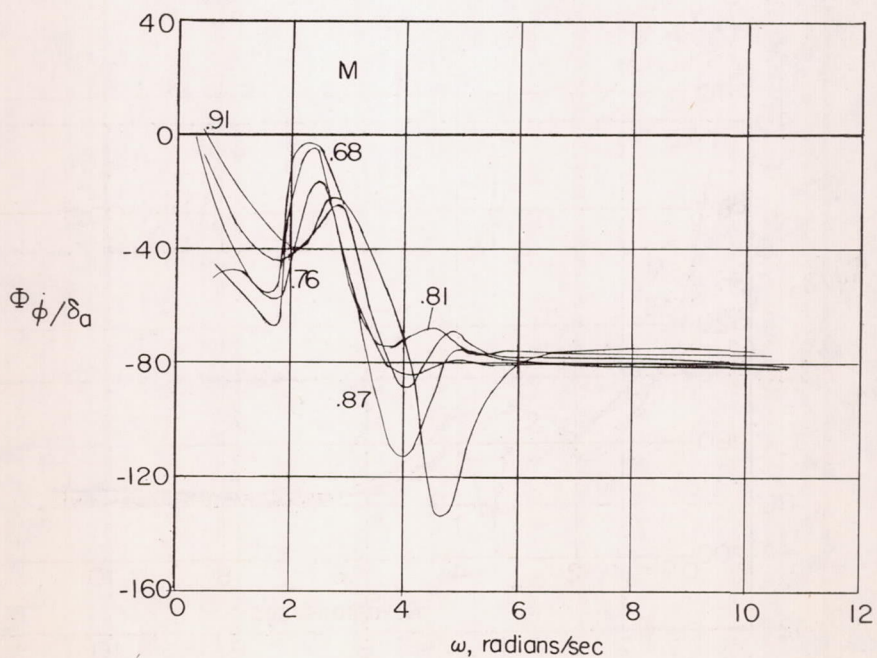
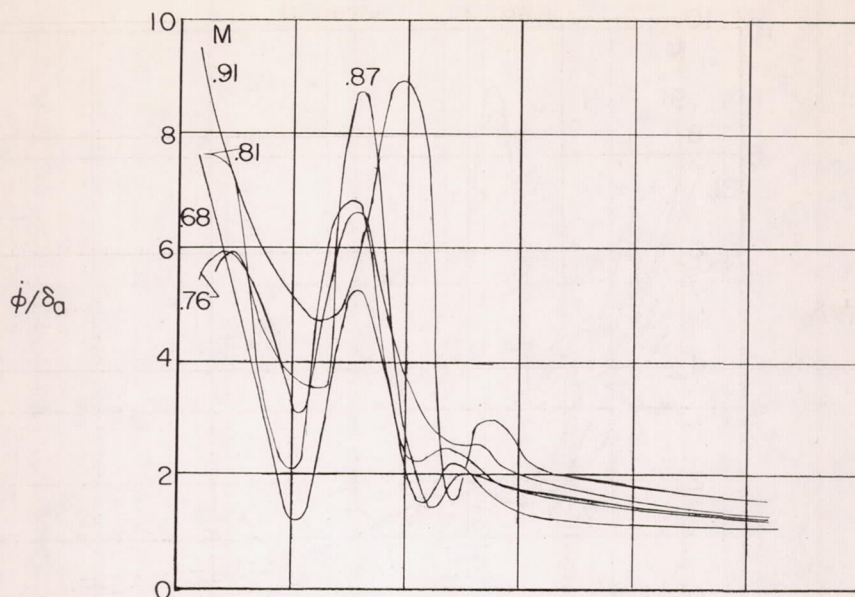
(c) Frequency response for left rudder pulses.

Figure 20.- Concluded.



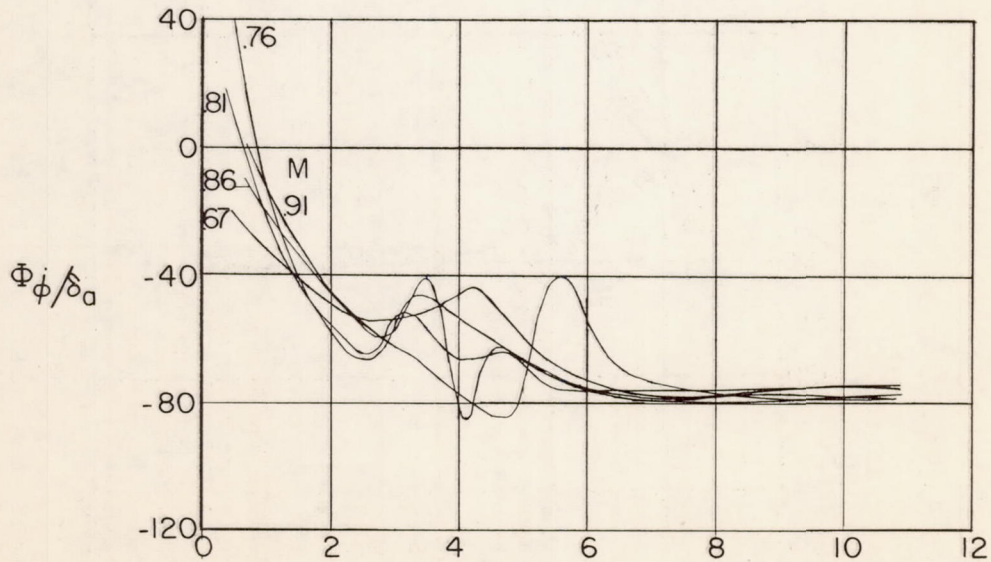
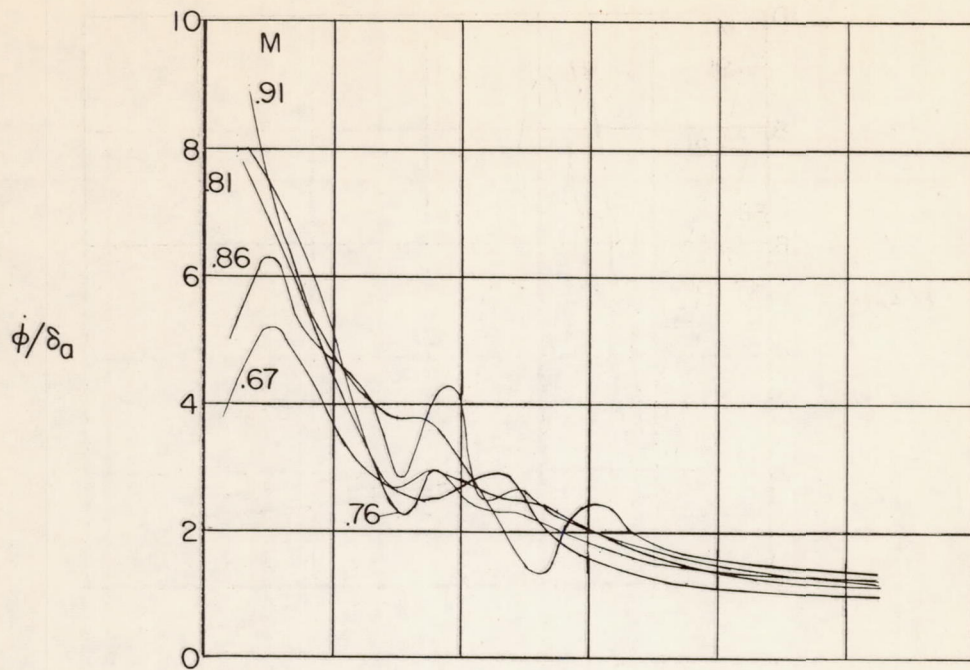
(a) Sample calculation showing calculated frequency response points at $M = 0.88$; $h_p = 40,000$ feet.

Figure 21.- Lateral frequency response $\dot{\Phi}/\delta_a$ as calculated from lateral transient responses.



(b) Frequency response for right aileron pulses.

Figure 21.- Continued.



(c) Frequency response for left aileron pulses.

Figure 21.- Concluded.

CONFIDENTIAL

CONFIDENTIAL